Highlights

The influence of circadian rhythms on CD8$^+$ T cell proliferation upon vaccination: a mathematical modeling perspective

Nasri Balit, Nicolas Cermakian, Anmar Khadra

- Potential targets of circadian rhythms within the ZAP70 signaling pathway were identified using bifurcation and sensitivity analyses.
- The level of vaccine load presented to a CD8$^+$ T cell was shown to dictate the effect of a circadian rhythm on its signaling response.
- The 'priming' effect of a circadian rhythm on CD8$^+$ T cell activation upon vaccination was demonstrated using time-series analyses.
- mTORC1 and its immediate upstream signaling molecules were shown to be regulated by circadian rhythms through independent mechanisms.

The influence of circadian rhythms on CD8$^+$ T cell proliferation upon vaccination: a mathematical modeling perspective

Nasri Balit[a], Nicolas Cermakian[b], Anmar Khadra[a,*]

[a]*Department of Physiology, McGill University, Montreal, Quebec, Canada*
[b]*Douglas Research Center, Department of Psychiatry, McGill University, Montreal, Quebec, Canada*

Abstract

Circadian rhythms have been implicated in the modulation of many physiological processes, including those associated with the immune system. For example, these rhythms influence CD8$^+$ T cell responses that are part of the adaptive immune system. The mechanism underlying this immune-circadian interaction, however, remains unclear, particularly in the context of vaccination. Here, we devise a molecularly-explicit gene regulatory network model of early signaling in naïve CD8$^+$ T cell activation pathway, comprised of three axes (or subsystems) labeled ZAP70, LAT and CD28, to elucidate the molecular details of this immune-circadian mechanism and its relation to vaccination. This is done by coupling the model to a periodic forcing function to identify the molecular players targeted by circadian rhythms, and analyzing how these rhythms subsequently affect CD8$^+$ T cell proliferation dynamics under differing levels of vaccine loads. By performing both bifurcation and parameter sensitivity analyses on the model at the single cell and population levels, we find that applying periodic forcing on molecular targets within the ZAP70 axis is sufficient to creating a day-night discrepancy in CD8$^+$ T cell activation in a manner that is dependent on the bistable switch inherent in CD8$^+$ T cell early signaling. We also demonstrate that the resulting CD8$^+$ T cell activation is dependent on the strength of the periodic coupling as

*Corresponding author.
Email addresses: nasri.balit@mail.mcgill.ca (Nasri Balit), nicolas.cermakian@mcgill.ca (Nicolas Cermakian), anmar.khadra@mcgill.ca (Anmar Khadra)

well as the vaccine load. Our results show that this day-night discrepancy is not transmitted to certain downstream molecules within the LAT subsystem, such as mTORC1, suggesting a secondary, independent circadian regulation on that molecule. We also corroborate experimental results by showing that the circadian rhythm primarily acts pre-vaccination, playing a facilitating role in priming $CD8^+$ T cells according to time of day. By applying population level analysis using bifurcation theory and by including all the hypothesized molecular targets of a circadian rhythm, we further demonstrate a variability between T cells (due to heterogeneity) induced by its circadian regulation, which may enhance the robustness of T cell responses to vaccination. This modeling study thus provides insights into the immune targets of the circadian clock, and proposes an interaction between vaccine strength and the influence of circadian rhythms on $CD8^+$ T cell proliferation.

Keywords: $CD8^+$ T cells, Adaptive immunity, Vaccination dynamics, Circadian rhythm, Mathematical modeling, Bifurcation analysis, Bistable switch, PRCC, Population level bistable switch
PACS: 0000, 1111
2000 MSC: 0000, 1111

---

1. Introduction

Circadian rhythms, 24 h cycles that modulates many of the body's internal processes (Portaluppi et al., 2012; de Goede et al., 2018), have been linked to the immune system from as far back as the 1960s (Halberg et al., 1960; Esquifino et al., 1996; Kawate et al., 1981; Young et al., 1995). This modulation is thought to be regulated by the presence of molecular clocks, made of clock genes, within cells of the immune system (Houtman et al., 2005; An et al., 2019; De Boer et al., 2001; Coombs et al., 2011; Bollinger et al., 2011; Cuesta et al., 2017; Boivin et al., 2003), including *Clock, Bmal1, Per1-3, Cry1-2*) (Cha et al., 2019). The expression level of these clock genes is regulated by transcription-translation feedback loops that create oscillations in their expression pattern with a $\sim$24 h period. These clock genes also interact with specific processes within the genome of immune cells and in turn modulate their expression in a cyclical manner, imposing circadian rhythms on them (Haspel et al., 2020; Labrecque and Cermakian, 2015; Jerigova et al., 2022). With evidence suggesting that circadian rhythms affects how the immune system responds to vaccination (Elliott et al., 1972; Long et al., 2016;

Phillips et al., 2008; de Bree et al., 2020), it becomes imperative to understand how this relation is manifested molecularly and dynamically at the single cell and population levels.

In innate immunity, the molecular basis of the immune-circadian link is relatively well-established with evidence indicating that these circadian interactions have links to specific processes within innate immune system (Haspel et al., 2020; Labrecque and Cermakian, 2015; Jerigova et al., 2022). Molecular clocks have been characterized in macrophages, neutrophils, eosinophils and natural killer (NK) cells (Keller et al., 2009). Specifically, in macrophages, the clock gene *REV-ERB*α has been shown to affect the inflammatory function of macrophages by repressing their NF-κB activation pathway (Sato et al., 2014; Wang et al., 2018), whereas in NK cells, mice with *Per2* knockdowns displayed reduced levels of proinflammatory cytokines, namely IFN-γ and IL-1β, after an LPS endotoxic shock (Liu et al., 2006). Furthermore, knockouts of *Bmal1* in myeloid cells, which make up the majority of innate immune cells, predispose mice to developing acute and chronic inflammation pathologies by disrupting the diurnal variation in monocyte number (Nguyen et al., 2013).

Although significant progress has been made in understanding how innate immunity is influenced by circadian rhythms, the molecular basis of this immune-circadian link remains unclear in adaptive immunity, particularly in CD8$^+$ effector T cell response. While circadian oscillations were observed in the RNA level of lymph node *Per2* and circulating naïve CD8$^+$ T cells (Fortier et al., 2011; Dimitrov et al., 2009), the molecular source(s) of this diurnic variation remains unknown. A recent transcriptomic study identified an increased activation of certain molecular players within the CD8$^+$ T cell activation pathway such as ZAP70, AKT and mTOR following a day-time vaccination, as well as an increased ability to combat an infectious challenge after a day-time vaccination (both compared to nigh-time vaccination) (Nobis et al., 2019). Moreover, another study has shown an increased level of ZAP70 prior to vaccination in the daytime (Fortier et al., 2011). These studies thus suggest that certain molecular players within the CD8$^+$ T cell activation signaling pathway interact with circadian rhythms in a way that primes these T cells to exhibit increased activation when vaccinated during the day-time compared to night-time; the details of this interaction, however, remains not fully explored.

In this study, we generate a theoretical framework, through mathematical modeling, to further elucidate the molecular basis of the immune-

circadian link in $CD8^+$ T cells following vaccination and its underlying dynamics. We adapted an experimentally validated, $CD4^+$ T cell gene regulatory model (Zheng et al., 2005; Perley et al., 2014) to simulate the immediate signaling events during naïve $CD8^+$ T cell activation following vaccination. By expanding the model to include a parameter-specific periodic forcing function, we explore the effects of a circadian rhythm on this signaling pathway to determine how it impacts $CD8^+$ T cell proliferation post-vaccination in a molecular-player-specific manner. This is first done via a single-parameter model framework, where bifurcation, sensitivity and time series analyses are performed one parameter at a time to develop a deeper understanding of the dynamics of this modulation. We will then expand this approach to a multi-parameter framework to generate more physiologically relevant conclusions about this system. While prior modeling studies have explored the effect of a circadian rhythm on the immune system (Bai and Zhou, 2012; Fan and Wang, 2010; Ji et al., 2010; Wang et al., 2006), these studies were not done using gene regulatory T cell models.

Through our single cell and population level modeling, we demonstrate the crucial role played by the ZAP70 axis (or subsystem) within the immune activation pathway in how a circadian rhythm exerts its effects in modulating $CD8^+$ T cell responses. By first highlighting the presence of a bistable switch in this subsystem, we show that this switch dictates the dynamics of the circadian modulation, and that the latter is dependent on both the vaccine load presented as well as on the magnitude of circadian coupling. Additionally, we establish that this modulation occurs prior to vaccination, suggesting a priming role for a circadian rhythm on $CD8^+$ T cell signaling. Interestingly, our results also reveal that downstream molecular players, such as mTORC1, require their own molecular clocks to produce oscillations, pointing to the existence of a complex, multi-layered circadian influence on $CD8^+$ T cell signaling. Our population modeling further expands on these ideas using a multi-parameter framework to produce more physiological conclusions about the influence of a circadian rhythm on $CD8^+$ T cell activation.

2. Single-cell model framework

2.1. Gene regulatory network model

To explore the dynamics of the circadian rhythm on $CD8^+$ T cell activation, a multi-scale gene regulatory network model of the early events of T cell

signaling is considered. The network model is described by a system of ordinary differential equations (ODEs) adapted from literature. This model, first developed in Zheng et al. (2005) and later extended in Perley et al. (2014), describes the immediate signaling events following antigenic stimulation of a single $CD4^+$ T cell. Because of the overlap in these early signaling events between $CD8^+$ and $CD4^+$ cells (Mørch et al., 2020), we have adapted the $CD4^4$ model to describe $CD8^+$ T cell signaling and modified it to exclude the gene regulatory output signals described in Perley et al. (2014) since $CD4^+$ and $CD8^+$ naïve T cells vary in their gene outputs (Hosking et al., 2014). The model is then coupled to a rhythmic signal representing the circadian rhythm and a single rate-activation parameter is chosen as a molecular target for circadian rhythm coupling. The effects of this coupling on model dynamics are subsequently analyzed.

Briefly, the gene regulatory network model is comprised of the early signaling events following T cell receptor (TCR) phosphorylation (Fig.1). According to this framework, a phosphorylated TCR (denoted by $TCRp$) binds to a tyrosine kinase ($ZAP70$) and triggers a cascade of interactions that ultimately result in the binding of $ZAP70$ to activated Src family protein kinases (SFK). This cascade of interactions is governed by a complex network of feedback mechanisms, regulated by positive feedback loops from the various forms of $ZAP70$ (denoted by $ZAP^*, ZAPp$ and SFK^*-$ZAPp$), as well as negative feedback loops from Src homology region 2 domain-containing phosphatase-1 ($SHP1$), C-terminal Src kinase (CSK), and CREB-binding protein (CBP). The activated $ZAPp$ and SFK^*-$ZAPp$ then feed into a series of reactions governed by various molecular players, such LAT, AKT etc., which ultimately result in the production of mammalian target of rapamycin complex 1 & 2 ($mTORC1$ and $mTORC2$). Both of these protein complexes, $mTORC1$ and $mTORC2$, are important in determining T cell fate and effector function (Chi, 2012). The rate equations and parameter values for this model are shown in Appendix 6.1, and a more detailed description can be found in Zheng et al. (2005) and Perley et al. (2014). Furthermore, a framework for this model is shown in Fig. 2 and a list of its parameter values are provided in Table 6.1.

2.2. The three key axes of the model

To explore the impact of the circadian rhythm on different components of the model, we divide the gene regulatory network model (Fig. 1) into three subsystems based on how they feed into each other. The first subsystem

(labeled the ZAP axis and highlighted by the red box in Fig. 1) includes the reactions that involve ZAP_{active} formation. It begins with the $TCRp$ input, and ends with $SFK*-ZAPp$ and $SHP1$. The second subsystem involves the signaling molecules downstream of ZAP_{active}, which include the reactions governing LAT phosphorylation (hence the label LAT axis highlighted by the blue box in Fig. 1). These reactions similarly do not receive feedback from downstream signaling molecules. Finally, the third subsystem involves the signaling molecules included in the $CD28$ signaling pathway (hence the label CD28 axis highlighted by the red box in Fig. 1)). It starts with the two input signals: ZAP_{active} and $CD28$, and ends with $mTORC1^*$. By exploring the effect of the circadian rhythm on the output of each one of these axes and determining how this circadian influence is filtered from one axis to the next, one can understand which one of them is more sensitive to circadian-induced perturbations, helping us identify potential molecular targets of the circadian rhythm.

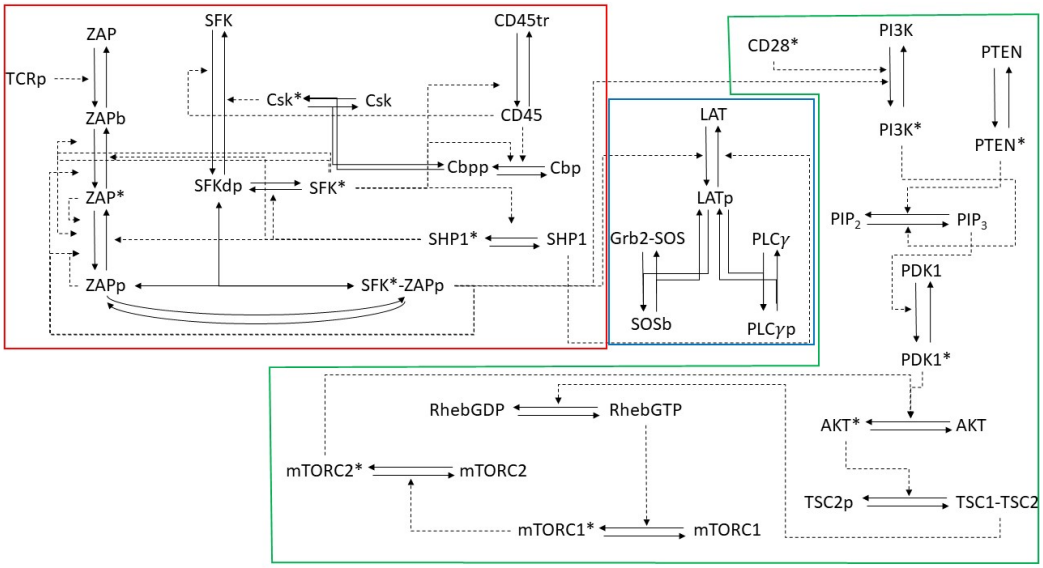

Figure 1: Schematic of the gene regulatory network adapted from Zheng et al. (2005) and Perley et al. (2014), and considered in our model framework to describe early signaling in $CD8^+$ T cells. The model can be divided into three main subsystems: the ZAP axis (red box), LAT axis (blue box) and CD28 axis (green box). Notice how the LAT and CD28 axes are linked to the ZAP axis in a feedforward manner without any feedback, and that the LAT and CD28 axes are similarly not linked in a feedforward manner. Asterisk is used to represent the active forms of the relevant molecules.

2.3. Periodic forcing by the circadian rhythm

To investigate the effect(s) of the circadian rhythm on T cell early signaling events, we incorporate a parameter-specific periodic forcing function applied on a given rate constant of one of these early signaling events; that is to say, an external forcing function is imposed onto a parameter of interest within the model, p_0, to produce a time-dependent variation in its value, denoted by p_t. This time-dependent variation in p_0 may get transmitted to downstream signals within the model, producing a time-dependent difference in its output signal. If so, this will allow us to identify which parameter(s) is/are responsible for the day-night discrepancy in $CD8^+$ T cell signaling. The equation we choose for this periodic forcing is given by

$$p_t = p_0 + p_0(\alpha_p \sin((2\pi/24)t + \beta_p)), \tag{1}$$

where p_0 is the default (original) value of the parameter p that is directly affected by the periodic forcing representing the circadian rhythm, t is time, α_p is the parameter-specific 'circadian coefficient' that determines how strongly that parameter is impacted by the oscillation, and β_p determines the parameter-specific phase shift of the oscillation.

According to Eqn. 1, the periodic forcing is defined as a sine function that is oscillating with a mean p_0 and a circadian coefficient α that represents the magnitude of circadian rhythm coupling to a specific parameter of interest. Such description allows us to study the effect of different strengths of circadian coupling on model dynamics. The choice of a sine function to describe the circadian rhythm is consistent with how it is routinely characterized in experimental literature (Elliott et al., 1972; Hickey et al., 1984; Naitoh et al., 1985).

To account for physiological limitations of how much a parameter can vary (see Appendix 6.3.2), we assume that $\alpha_p \in [0, 0.5]$. The periodic forcing defined in Eqn. 1 produces oscillations with a 24 h period and a phase shift of 0 for a positive feedback parameter and π for a negative feedback parameter; this reproduces the effect of the circadian rhythm, and leads to a variation in the signaling molecule associated with p_t, depending on time of day. Increasing the circadian coefficient α causes the amplitude of p_t to increase and thus the range of values of p_t to expand in a parameter-specific manner.

3. Outcomes of the single cell model

3.1. Strategy for identifying the molecular targets of the circadian rhythm

Identifying the parameters responsible for producing the key features of model dynamics will provide us with potential targets for producing the day-night variation in model output. By performing a dynamical systems analysis of the model, one can predict how parameter perturbations, due to the circadian rhythm, can modify model behaviour. To accomplish this, we make the assumption here that the circadian rhythm is primarily affecting the rate activation kinetics of signaling molecules within the $CD8^+$ T cell activation pathway. This is supported by the day-night discrepancy in active-forms of $CD8^+$ T cell signaling molecules shown in Nobis et al. (Nobis et al., 2019).

We begin first by performing parameter sweeps and bifurcation analyses within each axis of the gene regulatory network model to identify the broad signaling pathways defining the dynamics of our model. Once a 'key' axis is found, individual parameters within the axis are further explored using both parameter sensitivity and threshold analyses to identify targets for the circadian rhythm (i.e., periodic forcing).

3.1.1. The ZAP axis is pivotal in defining model dynamics

The ZAP axis is the most upstream subsystem of the model, receiving a direct $TCRp$ input and outputting various forms of activated ZAP: phosphorylated ZAP ($ZAPp$), active ZAP (ZAP^*), and active SFK-bound ZAP (SFK^*-$ZAPp$). To consolidate the various active forms of ZAP into a single indicator variable, we use the same approach as in Zheng et al. (2005) by defining a new output variable ZAP_{active} for this axis, given by

$$ZAP_{active} = \frac{(ZAPp + SFK^*\text{-}ZAPp)}{ZAP_{total}} \cdot 100, \tag{2}$$

where ZAP_{active} is the percentage of ZAP within a single T cell that has been fully phosphorylated, ZAPp and SFK*-ZAPp are the fully phosphorylated forms of ZAP70, and ZAP_{total} denotes the conserved total quantity of ZAP. With this output variable, the dynamics of the ZAP axis are explored through parameter sweeps and bifurcation analysis. In Fig. 2(A), we show that for $TCRp = 27000$ mol, the time course of ZAP_{active}, the output signal of the ZAP axis, changes significantly as the values of the rate activation parameters of the model are altered. For instance, as the rate activation parameter for

SHP1, $k10f$ (blue) decreases past a threshold of $\sim 4.7\ (\text{mol} \cdot \text{min})^{-1}$, the ZAP_{active} output jumps from 0 to a higher steady state of $\sim$25%. This threshold is also seen with other parameters within the model, as shown with $k4f$ (gray).

To further explore the dynamics of the model in more detail, a one-parameter bifurcation analysis of ZAP_{active} with respect to $k10f$ is conducted, as shown in Fig. 2(B). Branches of stable (unstable) steady states of the model are shown in red solid (gray dashed) lines. The gray dashed line exhibits loop points that represent saddle node bifurcations (SN1 and SN2). The stable and unstable branches are linked by Hopf bifurcations (HB1 and HB2) where envelopes of unstable limit cycles (blue dashed lines) emerge and terminate at homoclinic bifurcations (HM1 and HM2, respectively). As $k10f$ decreases, a jump in the ZAP_{active} steady state occurs upon crossing of the $HB2$ bifurcation point. We also note that there is a bistability region within which the two branches of stable steady states overlap (shown by the region where the two red solid lines cover the same range of $TCRp$ parameter values). This region is bounded by HB1 and HB2. Since the Hopf bifurcations produce envelopes of unstable limit cycles, periodic solutions are not observed when transitioning from one steady state to the other. Additionally, since the bistable regime is bounded by the two Hopf bifurcations HB1 and HB2, rather than the two saddle nodes $SN1$ & $SN2$, as typically seen in traditional bistable switches, the bistable regime and the hysteresis of the model are quite limited in range. This bifurcation diagram suggests that certain molecular players within the ZAP axis are quite important in modulating its response to a vaccine input; however, it remains unclear which specific parameters within the axis are most sensitive to perturbations in their values.

Extending this analysis to the LAT and CD28 axes indicates that their dynamics are not as complex. Indeed, parameter sweeps and bifurcation analyses reveal a monostable behaviour across all the parameters within these two subsystems, suggesting that the LAT and CD28 axes do not exert the same level of influence on the overall behaviour of the system as the ZAP axis. This is demonstrated in Fig. 2(C,E), where the time series simulations of $PLC\gamma p$ and $mTORC1^*$ percentages (relative to their individual total concentration) from the LAT and CD28 axes, respectively, are plotted at different parameter values of $k12f$ and $k13f$ (denoting the forward rates of LAT and $PLC\gamma$ phosphorylation, respectively) and at different parameter values of $k42f$ and $k43f$ (denoting the forward rates of $RhebGDP$ and $mTORC1$ activation, respec-

tively) provided in the legends; in these two cases, no threshold-dependent sudden jumps in their steady state output dynamics are observed. This is further confirmed in Fig. 2(D,F) showing a monotonically varying branch of stable equilibria in the bifurcation diagrams of $PLC\gamma p$ and $mTORC1^*$ precentages with respect to $k12f$ and $k42f$, respectively. This emphasizes the limited significance of these parameters in defining the dynamics of the LAT and CD28 axes output variables.

This result suggests that a circadian rhythm acting on signaling molecules within the ZAP axis would have the largest impact on model dynamics. This is validated in the next section when performing sensitivity analysis on the parameters of the ZAP axis.

3.1.2. Parameters of $ZAP70$ and $SHP1$ activation are the most sensitive to perturbation

To identify sensitive signaling molecules within the ZAP axis, partial rank correlation coefficient (PRCC) of each parameter within a given axis is calculated (Marino et al., 2008). A partial correlation characterizes the relationship between a parameter p_i and the output variable, while discounting the effects of other parameters in the model; this is repeated for every activation parameter p within the ZAP axis. This was done using a MATLAB package written by Marino et al. (Marino et al., 2008), which incorporates Latin Hypercube Sampling to generate parameter sets whose partial correlation coefficients are calculated. The results of this are shown in Fig. 3. From this plot, we designate $k4f, k5f, k8f2, k9f1$ and $k10f$ as sensitive parameters, i.e. with correlation coefficients $> |0.6|$. This threshold correlation coefficient represents 80% of the correlation coefficient of $k10f$ (whose correlation coeficient is 0.72), where $k10f$ denotes the rate of activation of the $SHP1$ molecule. Since $SHP1$ has been suggested to possess a circadian component in its regulation (Nobis et al., 2019), we assume that the other circadian-affected parameters of the model should posses a level of sensitivity equivalent or close to that possessed by $SHP1$ activation through $k10f$. Interestingly, those parameters identified with this approach are involved in the formation of ZAP_{active}, with $k4f$ and $k5f$ denoting the forward and backward rates of SFK^*-$ZAPp$ phosphorylation, and $k8f2$ and $k9f1$ denoting the formation rates of ZAP^* and $ZAPp$, respectively. Additionally, this sensitivity analysis demonstrates the importance of negative feedback in affecting ZAP_{active} through $SHP1^*$. Since $k10f$ was the primary negative feedback parameter implicated by this analysis, it will be our target param-

eter in the single-parameter analysis conducted in the following section.

3.2. The impact of vaccination on the steady state dynamics of the model

Implementing the periodic forcing function defined by Eqn. 1 on $k10f$ (the rate of activation of the $SHP1$ molecule) will allow this parameter to exhibit a 24 hr cycle, mimicking the influence of the circadian rhythm. This is shown in Fig. 4(A), where $k10f_t$ is plotted according to the circadian time of day, with $[0, 12]$ hr representing day-time and $[12, 24]$ hr representing night-time. The amplitude of this diurnal variation in $k10f_t$ varies according to α_{k10f} denoting the coefficient of variation; when $\alpha_{k10f} = 0.5$ (solid line), larger oscillations are produced compared to $\alpha_{k10f} = 0.25$ (dashed line). The respective day and night time maxima and minima of $k10f_t$ are identified by an orange (yellow) and blue (light blue) dot for each value of α_{k10f}, respectively. Recall that (see Fig. 2) the bifurcation diagram of the model exhibits a bistable switch with two saddle-nodes (SN1 and SN2) and two Hopf bifurcations (HB1 and HB2) at which two envelopes of unstable periodic orbits emerge and eventually terminate at homoclinic bifurcations (HM1 and HM2, respectively). Superimposing the orange and blue dots representing the maxima and minima of $k10f_t$ when $\alpha_{k10f} = 0.5$ on this bistable switch, as shown in Fig. 4(B), the orange dot ends up lying on the upper branch of stable equilibria (to the left of HB1), while the blue one ends up lying on the lower branch (to the right of HB2). This means that during a 24 hr day-night cycle in $k10f_t$, the solution trajectory of ZAP_{active} will oscillate between these two dots that represent the extrema of $k10f_t$ and cause it to jump back and forth between the two stable branches of equilibria. The jumping to the lower branch will occur during the transition from daytime to nighttime when the trajectory moves rightward along the upper branch of ZAP_{active} stable equilibria until it crosses HB1, leading the trajectory to jump to the lower stable branch and causing ZAP_{active} to decrease. Conversely, during the transition from nighttime to daytime, the trajectory will move leftward along the lower branch of ZAP_{active} stable equilibria until it crosses HB2, leading the trajectory to jump to the upper stable branch and causing ZAP_{active} to increase. Thus, the circadian rhythm on ZAP axis activation parameters can have a drastic effect on ZAP_{active} output. This drastic change in dynamics occurs because of the presence of the bistable switch with its two Hopf bifurcations: HB1 & HB2, lying within the parameter space afforded by $\alpha_{k10f} = 0.5$. This cycling between the two branches of equilibria every 12 hr suggests that the circadian rhythm can cause periodic oscillations in ZAP_{active} with large am-

plitudes. This then posses the question of how such mechanism interacts with vaccines?

To answer this question, we will first investigate how the impact of the circadian rhythm on T cell activation is affected by the $TCRp$ (the number of phosphorylated TCRs), which we assume to be an indicator of vaccine strength. This is done by considering two other values of $TCRp$: one that is higher than the one used in Fig. 4(A), namely, $TCRp = 40000$ mol, and another that is lower, i.e., $TCRp = 10000$ mol, and then plotting the one-parameter bifurcations of ZAP_{active} with respect to $k10f$ at these two $TRCp$ values as shown in Fig. 4(C,D), respectively. By superimposing the orange and blue dots representing the day and night extrema of $k10f_t$ when $\alpha_{k10f} = 0.5$ on these two bifurcation diagrams, we see that in both realizations, no Hopf or saddle node bifurcations end up separating the two dots to allow for drastic time-of-day dependent changes in ZAP_{active} seen in Fig. 4(B). Indeed, when $TCRp = 40000$ mol, the two dots become part of the upper branch of stable equilibria, producing an elevated output of ZAP_{active} independent of time of day, whereas when $TCRp = 10000$ mol, the inverse is seen, with the two dots lying on the lower branch of stable equilibria, producing baseline output of ZAP_{active} independent of time of day. Thus there seems to be an intermediate range of $TCRp$ within which the circadian rhythm can produce the largest day-night discrepancy in ZAP_{active}. This relationship between $TCRp$ and $k10f$ is further demonstrated by plotting the two-parameter bifurcation of ZAP_{active} with respect to both $TCRp$ and $k10f$ as shown in Fig. 4(E). The region bounded by the Hopf bifurcations (blue lines)demarcate the bistable regime, whereas the upper and lower regions denote the monostable elevated and baseline states of the model, respectively. Notice how the bistable regime shifts horizontally as the value of$TCRp$ is varied, indicating that there is an intermediate range of $TCRp$ within which the largest day-night discrepancy in ZAP_{active} can be generated. This means that the level of vaccines administered can alter $TCRp$ and cause the regime of bistability to shift accordingly.

Now that we have explored how vaccines may affect bistability with respect to $TCRp$ and $k10f$, we now examine how changing the the strength of the circadian rhythm through α_{k10f} can affect outcomes. By taking $TRCp = 27000$ mol and setting $\alpha_{k10f} = 0.25$ to produce the two extrema of $k10f_t$ identified by the yellow and light blue dots in Fig. 4(A), we find that superimposing these dots on the bifurcation diagram of ZAP_{active} with respect to α_{k10f} (see Fig. 4(F)) places them on the lower stable branch of equilibria.

According to this realization, solution trajectories are unable to cross the Hopf bifurcation HB2 and solely oscillate along this lower branch with very low amplitude, i.e., without exhibiting drastic day-night shift in ZAP_{active}. Such realization thus indicates that if the influence of the circadian rhythm is not strong enough, then an intermediate level of vaccination may still not be able to generate large amplitude day-night cycle in ZAP_{active}.

Taken together, these results thus demonstrate that the day-night discrepancy in signaling is dependent on both having a sufficiently large $TCRp$ input, as well as on possessing a sufficiently high α_{k10f}, such that the $k10f_t$ is able to cross HB1 and HB2 of the model. This further highlights the complex relationship between vaccine load and the strength of circadian modulation when mediating CD8$^+$ T cell response upon vaccination. Further experimental work is needed to validate the extent of this relationship.

3.3. Impact of circadian coupling on temporal evolution of CD8$^+$ T cell signaling

Now that we have determined the underlying steady state dynamics of circadian modulation of T cell activation upon vaccination, we now explore how the time series of the ZAP axis is affected by $k10f_t$ and the potential physiological implications of this on CD8$^+$ T cell signaling. To do so in the context of vaccination, we define two possible states that can be attained by the model: S_0 and S_1. S_0 represents the starting state of the model (pre-vaccination) and corresponds to a given initial amount of $TCRp$, assumed to be $TCRp_0 = 100$ mol; a nonzero basal level of $TRCp$ is chosen for this state to accommodate pMHC-TCR contacts with self or non-cognate antigens. S_1, on the other hand, denotes the post-vaccination state and corresponds to when $TCRp >> 10000$ mol ($>> TCRp_0$). The effect of the circadian rhythm on the time series of the ZAP axis in each of these states is then analyzed (see Fig. 5) by exploring the effects of a $k10f$-induced circadian rhythm on both S_0 or S_1.

Imposing a 24-hr circadian cycle on $k10f$ in the form of a sine wave with $\alpha_{k10f} = 0.5$ as in Fig. 5(A) and initiating model simulations from S_0 induce a repetitive very small-amplitude oscillations is ZAP_{active} (Fig. 5(B, inset)). Although $TRCp = 10000$ mol in Fig. 5(D), the monostable dynamics detected in this figure is responsible for generating these small amplitude oscillations that shuttle ZAP_{active} between the orange and blue dots. This is because the bifurcation diagram at S_0 is essentially the same as the one in Fig. 5(D). However, when vaccination is applied, the state of the system

switches to S_1. By setting $TCRp = 29000$ mol in S_1, ZAP_{active} then produces repetitive large amplitude oscillations regardless of the time of vaccination (Fig. 5(B,C)), with the daytime vaccination (at $t = 12$ hr) producing a faster response compared to the nighttime vaccination (at $t = 24$ hr). These large amplitude oscillations are reminiscent to those cycles between the orange and blue dots highlighted previously in Fig. 5(B); solution trajectories, in this case, cross the two Hopf bifurcations back and forth and jump between the branches of stable equilibria. Given that such oscillations indicate repetitive activation and deactivation of T cells, then this would preclude them from being physiological.

To address this latter issue, we hypothesize that upon vaccine application the effect of the circadian oscillations on $k10f$ is significantly attenuated with a much lower value for α_{k10f}. To test this hypothesis, we set $\alpha_{k10f} = 0$ right when vaccination is applied at both daytime (at $t = 12$ hr) and nighttime (at $t = 24$ hr) as shown in Fig. 5(D). This is done by freezing (i.e., fixing) the value of $k10f$ at its respective value upon vaccine onset. Even though vaccine application still transitions the system from the state S_0 to the state S_1, repetitive large amplitude oscillations no longer occur - only small amplitude oscillations in ZAP_{active} is seen prior to vaccination due to the circadian clock as described before for S_0. Interestingly, nighttime vaccination causes a very moderate increase in ZAP_{active} (Fig. 5(E)), whereas daytime vaccination causes a significant increase in ZAP_{active} (Fig. 5(F)), reaching a significantly elevated steady state due to the transition to the upper branch of stable equilibria highlighted in Fig. 5(B). The lack of oscillations in $k10f_t$ post vaccination prevents the solution trajectory from crossing HB1 and returning to the lower branch. These results thus corroborates the experimental finding that daytime vaccination is more effective in triggering T cell activation, and suggests that for this to be true, the diurnal effect of the circadian rhythm on early events of T cell signaling is significantly attenuated post vaccination. Taken together, these results indicate that the circadian rhythm primes or facilitates the activation of naïve $CD8^+$ T cells to produce the day-night discrepancy in ZAP_{active} output, rather than directly controlling it.

3.4. Characterizing the filtering properties of the ZAP axis

Throughout this study, we have explored the implications of the circadian rhythm on the ZAP axis, which we have found to be the primary driver of model dynamics with its intrinsic bistable switch. Here, we expand this study by exploring how the effects of the circadian rhythm acting directly on

the ZAP axis is transmitted to the downstream LAT and CD28 axes within the model in the absence of vaccination. Doing so would indicate whether a circadian rhythm within the ZAP axis is capable of producing a day-night discrepancy in the signaling of other downstream molecular players associated with these two axes. If not, this may suggest the presence of additional circadian clocks acting directly on these downstream signaling molecules.

To explore how the influence of the circadian oscillation within the ZAP axis in the absence of vaccination is transmitted to other axes of the model, we now consider the expanded model of Fig. 2 that includes the LAT and CD28 axes. In order to quantify how the circadian-dependent oscillations of $k10f_t$ are transmitted to other variables in these two axes , we will use the 'oscillatory contribution' ratio, ω_i, for every variable (molecular player) i of the model. This ω_i is defined as the relative effect of the oscillation in $k10f_t$ to the mean of the variable i at steady state. It is given by

$$\omega_i = 100 \times \frac{SS_{amp,i}}{SS_{mean,i}}, \tag{3}$$

where i represents the variable of interest, $SS_{amp,i}$ represents the amplitude of the steady state oscillations, and $SS_{mean,i}$ represents the mean of the variable. A larger ω_i indicates that a larger proportion of a variable's steady state can be explained by $k10f_t$, whereas a smaller ω_i indicates that the circadian-dependent oscillations in $k10f_t$ minimally alter the steady state of the variable i. To quantify ω_i, we will always assume that $k10f_t$ is oscillatory with a circadian coefficient of $\alpha_{k10f} = 0.5$.

By plotting the magnitude of ω_i for the major variables within the ZAP axis, as shown in Fig. 6(blue bar), we find that $SHP1_{active}$ is associated with the largest ω_{SHP1}, while the other variables (including $i = SFK^*, CSK^*, CBPp$) exhibit a reduced ω_i. This is expected since a periodic forcing on $k10f$ directly regulates SHP1 activation, altering $SHP1^*$. For the variables within the LAT axis, on the other hand, Fig. 6(B) shows that the magnitude of ω_i ($i = LATp, PLC\gamma p, SOSb$) are lower than those for the key molecular players within the ZAP axis: ZAP_{active} and $SHP1^*$, suggesting that some of the $k10f$-induced oscillation is filtered out between axes. However, the oscillations remain identifiable within the axis, indicating that a circadian rhythm in the ZAP axis is sufficiently transmitted to the LAT axis. Interestingly, in the CD28 axis, Fig. 6(C) shows that while the oscillation from $k10f_t$ is adequately transmitted to many of the signaling molecules (including $i = PI3K^*, PDK1^*, AKT^*, mTORC2^*$) with moderate values of ω_i,

it is completely filtered out when $i = TSC1-2, RhebGTB, mTORC1^*$ (i.e., $\omega_i = 0$ for all of these cases). This suggests that oscillations in $k10f_t$ directly influencing the ZAP axis may not be able to produce the experimentally observed oscillations within $mTORC1^*$ and its immediate precursors (Nobis et al., 2019), despite producing them in the other signaling molecules of this axis.

This was resolved by imposing a periodic forcing component, representing the influence of the circadian rhythm, directly on $RhebGTP$ activation parameter $k42f$ with $\alpha_{k42f} = 0.5$; this resulted in a high $\omega_{RhebGTP}$ and $\omega_{mTORC1_{active}}$ of 49% and 49.5%, respectively, as shown in Fig. 6(C, inset). Curiously, adding a periodic forcing onto any of the more upstream signaling molecules within the CD28 axis, such as AKT, PI3K or even TSC1-2, was not able to produce oscillations in $RhebGTP$ and $mTORC1^*$, further indicating the presence of an independent circadian regulation of $RhebGTP$ and $mTORC1^*$. Since $S6$ (a molecular derivative of $mTORC1$), has been experimentally shown to have a circadian-influenced day-night discrepancy (Nobis et al., 2019), these modeling results suggest that a circadian rhythm within the ZAP axis may not be sufficient to explain these downstream oscillations, pointing to a potential secondary molecular clock acting directly on the gene transcripts of $mTORC1$-related players.

4. Population model framework

To better understand T cell responses to circadian oscillations and vaccines, it is imperative to obtain a broader view of model dynamics at the population level. We do so by simulating the steady state dynamics of $k = 100$ model realizations of the ZAP axis, each with a randomly selected parameterization of the model. This is done after eliminating the oscillatory solutions using a method called parallel coordinate plot (see Appendix 6.3).

We initially conduct this parameterization by first targeting one parameter, namely, $k10f_k$. This is done by randomly assigning random values for this parameter within the range $[0.5 \times k10f_0, 1.5 \times k10f_0]$ for each model realization k, where $k10f_0$ denotes the default parameter value of $k10f$ listed in Table 6.1. Doing so generates heterogeneity between each model realization through this parameter. These model realizations are then all integrated from the same initial conditions at increasing values of $TRCp \in [1, 3.5] \cdot 10^4$ mol and the steady state values of ZAP_{active} are plotted with respect to $TRCp$ (along the x-axis) as shown in Fig. 7(A). Each point on the graph denotes

the steady state ZAP_{active} at a certain parameter value of $k10f_k$ within the previously defined range. This provides a snapshot of 100 steady states of the model, each at a different circadian time defined by the value of $k10f_k \in [0.5 \times k10f_0, 1.5 \times k10f_0]$ (recall that we assumed the circadian rhythm affects the value of $k10f$ when we defined $k10f_t$). Plotting the steady states of these 100 realizations with respect to $TCRp$, the surrogate for vaccine strength, highlights how the model output varies under differing vaccine loads. This produces what looks like a one-parameter bifurcation diagram that encompasses not only the effects of the circadian rhythm on T cell activation through $k10f$, but also the effects of vaccine strength through $TRCp$. We refer to this plot as a 'macro-bifurcation' diagram.

According to this macro-bifurcation diagram, we can split the parameter space of the model into 3 regions labeled insensitive, sensitive and elevated. This distinction depends on the distribution of ZAP_{active} at each value $TCRp$. The insensitive region is the range of $TCRp \in [1, 2] \cdot 10^4$ mol, where ZAP_{active} is purely in its inactive state, regardless of the parameterization of $k10f$. The sensitive region, on the other hand, corresponds to the range of $TCRp \in [2, \sim 3.10] \cdot 10^4$ mol, where ZAP_{active} can be either elevated or not, depending on the value of the parameter $k10f_t$. We denote this region as possessing 'macro-bistability', as the magnitude of its output depends on the value of the circadian-affected parameter $k10f$. Finally, the elevated region is the one that corresponds to the range $TCRp \in [\sim 3.10, 3.5] \cdot 10^4$ mol, where ZAP_{active} is purely elevated, regardless of the value of $k10f_t$.

Unique to the macro-bifurcation diagram is the ability to expand this analysis to n parameters, whereas our previous analysis was limited to 1 or 2 dimensions using the one and two-parameter bifurcations. Indeed, by expanding this approach to include variability in the positive feedback parameters $k4f, k9f1$, negative feedback parameters $k7f, k10f, k11f$ and our manually derived threshold parameter $k8f1$ ((see Appendix 6.3.2)) as shown in Fig. 7(B), we can obtain macro-bifurcation diagram of ZAP_{active} with respect to $TCRp \in [0.5, 5.5] \cdot 10^4$ mol. We have chosen these parameters because they can act as possible molecular targets of the circadian rhythm in early $CD8^+$ T cell signaling and because they were a subset of 'sensitive' parameters identified by our sensitivity analysis of Fig. 3 (for the full definition of $k4f, k9f1, k7f, k10f, k11f, k8f1$, please see Tables 6.1). Combining their effects in a macro-bifurcation diagram can thus provide a more physiological understanding of how the circadian rhythm can impact $CD8^+$ T cell activation. Simulating 100 realizations of the model, by randomly sampling these

parameters from their respective ranges defined by $[0.5 \times par_0, 1.5 \times par_0]$, where $par = k4f, k9f1, k7f, k10f, k11f, k8f1$ and par_0 is the default parameter value of each one of them (see Tables 6.1), and plotting the steady state values of ZAP_{active} produced by the model with respect to $TCRp$ produces the macro-bifurcation diagram shown in Fig. 7(B). Although the distinction between insensitive, sensitive and elevated regions remains regardless of the number of parameters included (the elevated region is past our pre-defined range for $TCRp$), the macro-bistable region of the model (the sensitive region) becomes more expanded (i.e., more robust) compared to that shown in Fig. 7(A): $TCRp \in [2, 3] \cdot 10^4$ mol in panel (A) vs $TCRp \in [2, 4] \cdot 10^4$ in panel (B). This demonstrates that our theoretical framework is maintained when adding additional parameters, and can provide insights into how adding additional parameters to our macro-bifurcation analysis may affect early $CD8^+$ T cell signaling in response to vaccines. Further analysis, coupled with experimental work, may help determine how additional rate activation parameters can alter the macro-bifurcation diagram, providing a more targeted approach to explore the effects of the circadian rhythm on $CD8^+$ T cell activation.

5. Discussion

In this study, we provided detailed analysis of the dynamics of the signaling molecules involved in producing the day-night discrepancy seen in early $CD8^+$ T cell signaling. Additionally, we explored how this day-night discrepancy may be altered by vaccines of different strengths. This was done through a mathematical modeling approach, which provided flexibility in studying how changes in rate activation parameters can affect $CD8^+$ T cell activation.

More specifically, a reference model for $CD4^+$ T cell activation obtained from Zheng et al. (2005); Perley et al. (2014) was adapted to $CD8^+$ T cell activation and used to conduct our analysis. This model was then split into 3 subsystems, and a dynamical systems analysis was conducted on each one to identify the main drivers of model dynamics. Through this analysis, the subsystem associated with $ZAP70$ activation (ZAP axis) was shown to drastically affect the dynamics of the other two downstream LAT and CD28 axes by uniquely possessing a bistable switch. This is in agreement with prior modeling literature suggesting a bistability within ZAP70 signaling (Lipniacki et al., 2008). To further pinpoint potential molecular targets of the circadian rhythm within the ZAP axis, a global sensitivity analysis was conducted using Latin hypercube sampling and partial rank correlation

coefficient (Marino et al., 2008). This was done to identify how parameter perturbations within the ZAP axis can affected the dynamics of its output signal, namely ZAP_{active}. Since the circadian rhythm was implemented in a parameter-specific manner, identifying the most sensitive parameters of the model provided insights into potential targets of the circadian clock in $CD8^+$ T cell signaling. Through this analysis, we identified that $ZAP70$ and $SHP1$ activation parameters, namely $k4f, k5f, k10f, k9f1, k8f2$ were the most sensitive to perturbations, conclusions that are aligned with the results of transcriptomic analyses of $CD8^+$ T cells in mouse genomes (Nobis et al., 2019).

To analyze the effects of this parameter-specific circadian coupling on model dynamics, a single-parameter bifurcation analysis approach was applied. Due to the bistable switch within the ZAP axis, we showed that, for a given vaccine input $TCRp$, an elevated ZAP_{active} was dependent on the value of the circadian-coupled bifurcation parameter $k10f_t$, especially relative to its Hopf bifurcation points, thus producing a day-night discrepancy. This day-night discrepancy was also shown to be affected by the vaccine load presented to the system, via the input parameter $TCRp$. This suggests a dependency between the vaccine load presented to $CD8^+$ T cells and the influence of the circadian rhythm, in such a way that there exists a threshold in $TCRp$ below of which the circadian rhythm may not affect $CD8^+$ T cell signaling. These results suggest a complex relationship between vaccine load and circadian coupling, which may explain why characterizing the vaccination effects of circadian rhythm in T cells has been relatively difficult thus far.

Through a time-series analysis on the single-cell scale, we showed that only a circadian rhythm in the S_0 state of the model produces a physiologically valid day-night discrepancy and that such circadian effect must abort post vaccination. This suggests that the physiological circadian rhythm may act during the pre-vaccination state of a $CD8^+$ T cell, 'priming' them to respond to a vaccine. This result corroborates previously observed experimental results showing that $CD8^+$ T cells are more primed for activation even prior to vaccination (Nobis et al., 2019). Additionally, this finding is aligned with research in macrophages showing that the $Bmal1$ clock gene expression is reduced after an immune challenge via LPS (Curtis et al., 2015).

To expand this analysis to other molecular players of $CD8^+$ T cell signaling, the filtering properties of molecular players within the ZAP axis to the downstream LAT and CD28 axes were explored. Our results re-

vealed that an S_0 circadian rhythm within the ZAP axis is not transmitted to certain downstream signaling molecules within the CD28 axis, namely $TSC1-2, RhebGTP$ & $mTORC1$. However, a circadian rhythmicity to their activity was restored by adding a circadian component to their own activation parameters, namely to $k42f$. Since a day-night discrepancy was experimentally observed in $mTORC1^*$ (Nobis et al., 2019), our results suggest that this day-night discrepancy may be due to a secondary, independent molecular clock acting directly on $mTORC1$, rather than being due to the activity of the upstream molecular clock within the ZAP axis.

To produce a more physiological representation of $CD8^+$ T cell responses to vaccination and how that is impacted by circadian rhythm, we implemented a multi-dimensional population level modeling approach. This allowed us to explore the effect of the circadian rhythm on multiple molecular players simultaneously, as well as determine how heterogeneity in $CD8^+$ T cell population affect their robustness to vaccination. Through these simulations, three regions of activity with respect to vaccine load defined by $TCRp$ were identified when key circadian-dependent parameters were randomly sampled within their respective ranges: insensitive, sensitive (macro-bistable) and elevated. This macro-bifurcation diagram may provide a framework to explore the results of adding a circadian perturbation to additional molecular players with the purpose of motivating further experimental research.

One limitation of this study is its assumption that changes in activated ZAP70 and mTOR translate to changes in $CD8^+$ T cell proliferation. Our future work involves expanding this model to cover the downstream $CD8^+$ gene regulatory outputs. This would expand the scope of the model and allow us to make direct predictions about cytokine production and subsequent proliferation of $CD8^+$ T cells. This expansion would also assist in the experimental validation of the model, since outcomes would be closely linked to $CD8^+$ T cell responses. Alternatively, a different reference model may be chosen as a starting point for this analysis using previously proposed mathematical models of T cell signaling Lipniacki et al. (2008); De Boer et al. (2001, 2003); Coombs et al. (2002); François et al. (2013). That said, this study provided several novel insights into the effect of the circadian rhythm on $CD8^+$ T cell signaling, in the context of vaccination, and serves a valid framework for assessing the influence of the circadian rhythm in other models.

Acknowledgments

This work was supported by the Natural Sciences and Engineering Council of Canada (http://www.nserc-crsng.gc.ca/index_eng.asp) discovery grant to A.K. and the Canadian Institutes of Health Research (https://cihr-irsc.gc.ca/e/193.html) grants program: MOP-119322 and PJT-186278 to N.C. N.B. was supported by the Canada Graduate Scholarships — Master's program (https://www.nserc-crsng.gc.ca/students-etudiants/pg-cs/cgsm-bescm_eng.asp).

References

An, W., Park, K., Reyes, A., Kwieraga, A., Sabri, N., Frey, A., Chronopoulou, E., Savas-Carstens, J., Soper, D., Elia, J., et al., 2019. The phosphorylation kinetics of the key regulators in T cell receptor signaling pathway.

Bai, Z., Zhou, Y., 2012. Dynamics of a viral infection model with delayed CTL response and immune circadian rhythm. Chaos, Solitons and Fractals 45, 1133–1139. URL: https://www.sciencedirect.com/science/article/pii/S0960077912001245, doi:https://doi.org/10.1016/j.chaos.2012.06.001.

Boivin, D.B., James, F.O., Wu, A., Cho-Park, P.F., Xiong, H., Sun, Z.S., 2003. Circadian clock genes oscillate in human peripheral blood mononuclear cells. Blood 102, 4143–4145.

Bollinger, T., Leutz, A., Leliavski, A., Skrum, L., Kovac, J., Bonacina, L., Benedict, C., Lange, T., Westermann, J., Oster, H., et al., 2011. Circadian clocks in mouse and human cd4+ t cells. PloS one 6, e29801.

de Bree, L.C.J., Mourits, V.P., Koeken, V.A., Moorlag, S.J., Janssen, R., Folkman, L., Barreca, D., Krausgruber, T., Fife-Gernedl, V., Novakovic, B., et al., 2020. Circadian rhythm influences induction of trained immunity by bcg vaccination. The Journal of clinical investigation 130, 5603–5617.

Cha, H.K., Chung, S., Lim, H.Y., Jung, J.W., Son, G.H., 2019. Small molecule modulators of the circadian molecular clock with implications for neuropsychiatric diseases. Frontiers in Molecular Neuroscience 11. URL: https://www.frontiersin.org/article/10.3389/fnmol.2018.00496, doi:10.3389/fnmol.2018.00496.

Chi, H., 2012. Regulation and function of mtor signalling in t cell fate decisions. Nature reviews immunology 12, 325–338.

Coombs, D., Dushek, O., Merwe, P., 2011. A review of mathematical models for T cell receptor triggering and antigen discrimination. Mathematical models and immune cell biology , 25–45.

Coombs, D., Kalergis, A.M., Nathenson, S.G., Wofsy, C., Goldstein, B., 2002. Activated tcrs remain marked for internalization after dissociation

from pmhc. Nature Immunology 3, 926–931. URL: https://doi.org/10.1038/ni838, doi:10.1038/ni838.

Cuesta, M., Boudreau, P., Cermakian, N., Boivin, D.B., 2017. Rapid resetting of human peripheral clocks by phototherapy during simulated night shift work. Scientific reports 7, 1–11.

Curtis, A.M., Fagundes, C.T., Yang, G., Palsson-McDermott, E.M., Wochal, P., McGettrick, A.F., Foley, N.H., Early, J.O., Chen, L., Zhang, H., et al., 2015. Circadian control of innate immunity in macrophages by miR-155 targeting Bmal1. Proceedings of the National Academy of Sciences 112, 7231–7236.

De Boer, R.J., Homann, D., Perelson, A.S., 2003. Different dynamics of CD4+ and CD8+ T cell responses during and after acute lymphocytic choriomeningitis virus infection. The Journal of Immunology 171, 3928–3935.

De Boer, R.J., Oprea, M., Antia, R., Murali-Krishna, K., Ahmed, R., Perelson, A.S., 2001. Recruitment times, proliferation, and apoptosis rates during the CD8+ T-cell response to lymphocytic choriomeningitis virus. Journal of virology 75, 10663–10669.

Dimitrov, S., Benedict, C., Heutling, D., Westermann, J., Born, J., Lange, T., 2009. Cortisol and epinephrine control opposing circadian rhythms in t cell subsets. Blood, the Journal of the American Society of Hematology 113, 5134–5143.

Elliott, A.L., Mills, J., Minors, D., Waterhouse, J., 1972. The effect of real and simulated time-zone shifts upon the circadian rhythms of body temperature, plasma 11-hydroxycorticosteroids, and renal excretion in human subjects. The Journal of Physiology 221, 227–257.

Esquifino, A.I., Selgas, L., Arce, A., Maggiore, V.D., Cardinali, D.P., 1996. Twenty-four-hour rhythms in immune responses in rat submaxillary lymph nodes and spleen: effect of cyclosporine. Brain Behav Immun 10, 92–102. doi:10.1006/brbi.1996.0010.

Fan, A., Wang, K., 2010. A viral infection model with immune circadian rhythms. Applied Mathematics and Computation 215,

3369–3374. URL: https://www.sciencedirect.com/science/article/pii/S0096300309009333, doi:https://doi.org/10.1016/j.amc.2009.10.028.

Fortier, E.E., Rooney, J., Dardente, H., Hardy, M.P., Labrecque, N., Cermakian, N., 2011. Circadian variation of the response of T cells to antigen. J Immunol 187, 6291–300. doi:10.4049/jimmunol.1004030.

François, P., Voisinne, G., Siggia, E.D., Altan-Bonnet, G., Vergassola, M., 2013. Phenotypic model for early t-cell activation displaying sensitivity, specificity, and antagonism. Proceedings of the National Academy of Sciences 110, E888–E897.

de Goede, P., Wefers, J., Brombacher, E.C., Schrauwen, P., Kalsbeek, A., 2018. Circadian rhythms in mitochondrial respiration. J Mol Endocrinol 60, R115–r130. doi:10.1530/jme-17-0196.

Halberg, F., Johnson, E.A., Brown, B.W., Bittner, J.J., 1960. Susceptibility rhythm to e. coli endotoxin and bioassay. Proceedings of the Society for Experimental Biology and Medicine 103, 142–144.

Haspel, J.A., Anafi, R., Brown, M.K., Cermakian, N., Depner, C., Desplats, P., Gelman, A.E., Haack, M., Jelic, S., Kim, B.S., et al., 2020. Perfect timing: circadian rhythms, sleep, and immunity—an nih workshop summary. JCI insight 5.

Hickey, D., Kirkland, J., Lucas, S., Lye, M., 1984. Analysis of circadian rhythms by fitting a least squares sine curve. Computers in biology and medicine 14, 217–223.

Hosking, M.P., Flynn, C.T., Whitton, J.L., 2014. Antigen-specific naive cd8+ t cells produce a single pulse of ifn-γ in vivo within hours of infection, but without antiviral effect. The Journal of Immunology 193, 1873–1885.

Houtman, J.C., Houghtling, R.A., Barda-Saad, M., Toda, Y., Samelson, L.E., 2005. Early phosphorylation kinetics of proteins involved in proximal TCR-mediated signaling pathways. The Journal of Immunology 175, 2449–2458.

Jerigova, V., Zeman, M., Okuliarova, M., 2022. Circadian disruption and consequences on innate immunity and inflammatory response. International Journal of Molecular Sciences 23, 13722.

Ji, Y., Min, L., Zheng, Y., Su, Y., 2010. A viral infection model with periodic immune response and nonlinear CTL response. Mathematics and Computers in Simulation 80, 2309–2316. URL: https://www.sciencedirect.com/science/article/pii/S0378475410001539, doi:https://doi.org/10.1016/j.matcom.2010.04.029.

Kawate, T., Abo, T., Hinuma, S., Kumagai, K., 1981. Studies of the bioperiodicity of the immune response. II. Co-variations of murine T and B cells and a role of corticosteroid. The Journal of Immunology 126, 1364. URL: http://www.jimmunol.org/content/126/4/1364.abstract.

Keller, M., Mazuch, J., Abraham, U., Eom, G.D., Herzog, E.D., Volk, H.D., Kramer, A., Maier, B., 2009. A circadian clock in macrophages controls inflammatory immune responses. Proceedings of the National Academy of Sciences 106, 21407–21412. URL: https://www.pnas.org/doi/abs/10.1073/pnas.0906361106, doi:doi:10.1073/pnas.0906361106.

Labrecque, N., Cermakian, N., 2015. Circadian clocks in the immune system. J Biol Rhythms 30, 277–90. doi:10.1177/0748730415577723.

Lipniacki, T., Hat, B., Faeder, J.R., Hlavacek, W.S., 2008. Stochastic effects and bistability in T cell receptor signaling. Journal of Theoretical Biology 254, 110–122. URL: https://www.sciencedirect.com/science/article/pii/S0022519308002208, doi:https://doi.org/10.1016/j.jtbi.2008.05.001.

Liu, J., Mankani, G., Shi, X., Meyer, M., Cunningham-Runddles, S., Ma, X., Sun, Z.S., 2006. The circadian clock period 2 gene regulates gamma interferon production of nk cells in host response to lipopolysaccharide-induced endotoxic shock. Infection and immunity 74, 4750–4756.

Long, J.E., Drayson, M.T., Taylor, A.E., Toellner, K.M., Lord, J.M., Phillips, A.C., 2016. Morning vaccination enhances antibody response over afternoon vaccination: a cluster-randomised trial. Vaccine 34, 2679–2685.

Marino, S., Hogue, I.B., Ray, C.J., Kirschner, D.E., 2008. A methodology for performing global uncertainty and sensitivity analysis in systems biology. Journal of theoretical biology 254, 178–196.

Mørch, A.M., Bálint, Š., Santos, A.M., Davis, S.J., Dustin, M.L., 2020. Coreceptors and tcr signaling–the strong and the weak of it. Frontiers in cell and developmental biology 8, 597627.

Naitoh, P., Englund, C.E., Ryman, D.H., 1985. Circadian rhythms determined by cosine curve fitting: analysis of continuous work and sleep-loss data. Behavior Research Methods, Instruments, & Computers 17, 630–641.

Nguyen, K.D., Fentress, S.J., Qiu, Y., Yun, K., Cox, J.S., Chawla, A., 2013. Circadian gene bmal1 regulates diurnal oscillations of ly6chi inflammatory monocytes. Science 341, 1483–1488.

Nguyen, L.K., Degasperi, A., Cotter, P., Kholodenko, B.N., 2015. DYVIPAC: an integrated analysis and visualisation framework to probe multidimensional biological networks. Scientific Reports 5, 12569. URL: https://doi.org/10.1038/srep12569, doi:10.1038/srep12569.

Nobis, C.C., Dubeau Laramée, G., Kervezee, L., Maurice De Sousa, D., Labrecque, N., Cermakian, N., 2019. The circadian clock of CD8 T cells modulates their early response to vaccination and the rhythmicity of related signaling pathways. Proceedings of the National Academy of Sciences 116, 20077. URL: http://www.pnas.org/content/116/40/20077.abstract, doi:10.1073/pnas.1905080116.

Perley, J.P., Mikolajczak, J., Buzzard, G.T., Harrison, M.L., Rundell, A.E., 2014. Resolving early signaling events in T-cell activation leading to IL-2 and FOXP3 transcription. Processes 2, 867–900. URL: https://www.mdpi.com/2227-9717/2/4/867.

Phillips, A.C., Gallagher, S., Carroll, D., Drayson, M., 2008. Preliminary evidence that morning vaccination is associated with an enhanced antibody response in men. Psychophysiology 45, 663–666.

Portaluppi, F., Tiseo, R., Smolensky, M.H., Hermida, R.C., Ayala, D.E., Fabbian, F., 2012. Circadian rhythms and cardiovascular health. Sleep Med Rev 16, 151–66. doi:10.1016/j.smrv.2011.04.003.

Sato, S., Sakurai, T., Ogasawara, J., Shirato, K., Ishibashi, Y., Oh-ishi, S., Imaizumi, K., Haga, S., Hitomi, Y., Izawa, T., et al., 2014. Direct and indirect suppression of interleukin-6 gene expression in murine macrophages by nuclear orphan receptor rev-erbα. The Scientific World Journal 2014.

Wang, K., Wang, W., Liu, X., 2006. Viral infection model with periodic lytic immune response. Chaos, Solitons and Fractals 28, 90–99. URL: https://www.sciencedirect.com/science/article/pii/S0960077905004881, doi:https://doi.org/10.1016/j.chaos.2005.05.003.

Wang, S., Lin, Y., Yuan, X., Li, F., Guo, L., Wu, B., 2018. Rev-erbα integrates colon clock with experimental colitis through regulation of nf-κb/nlrp3 axis. Nature communications 9, 1–12.

Young, M.R.I., Matthews, J.P., Kanabrocki, E.L., Sothern, R.B., Roitman-Johnson, B., Scheving, L.E., 1995. Circadian rhythmometry of serum Interleukin-2, Interleukin-10, Tumor Necrosis Factor-α, and Granulocyte-Macrophage Colony-Stimulating factor in men. Chronobiology International 12, 19–27. URL: https://doi.org/10.3109/07420529509064496, doi:10.3109/07420529509064496.

Zheng, Y., Balakrishnan, V., Buzzard, G., Geahlen, R., Harrison, M., Rundell, A., 2005. Modeling and analysis of early events in T-lymphocyte antigen-activated intracellular-signaling pathways. Journal of Computational and Applied Mathematics 184, 320–341. URL: https://ui.adsabs.harvard.edu/abs/2005JCoAM.184..320Z.

6. Appendix

6.1. Model Parameterization

Here, we discuss the key reactions and framework of the model as well as note any modifications made by us to accommodate $CD8^+$ T cell signaling. Broadly. the model encompasses the immediate events following antigen presentation, on a single T cell scale. The equations of the model are shown in Table 2.

Variable	Differential Equation
ZAP axis	
$ZAPb$	$r1 - r8$
ZAP^*	$r8 - r9$
$ZAPp$	$r9 - r4 + r5$
SFK^*-$ZAPp$	$r4 - r5$
$SFKdp$	$r2 - r3 - r4$
SFK^*	$r3 + r5$
$CD45tr$	$r11$
$CBPp$	$r6 - r7$
CSK^*	$r7$
$SHP1^*$	$r10$
LAT axis	
$LATp$	$r11 - r12 - r13$
$SOSb$	$r12$
$PLC\gamma p$	$r13$
CD28 axis	
$PI3K^*$	$r14$
$PTEN^*$	$r22$
PIP_3	$r15$
$PDK1^*$	$r16$
AKT^*	$r17$
$TSC2p$	$-r18$
$RhebGDP$	$-r19$
$mTORC1^*$	$r20$
$mTORC2^*$	$r21$

Table 1: Differential equations of the various signaling molecules within the model. Equations adapted from Zheng et al. (2005) and Perley et al. (2014).

Rate Equation	Components
	ZAP axis
$r1$	$(k1f(2TCRp - ZAPb - ZAP^* - ZAPp - SFK^*\text{-}ZAPp)ZAP - k1r\,ZAPb) * 60$
$r2$	$(k2f\,CD45\,SFK - k2r\,CSK^*\,SFKdp) * 60$
$r3$	$(k3f\,SFKdp - (k3r1\,SHP1^* + k3r2)SFK^*) * 60$
$r4$	$(k4f\,SFK^*\text{-}ZAPp\,SFKdp - k4r\,SFK^*\text{-}ZAPp) * 60$
$r5$	$(k5f\,SFK^*\text{-}ZAPp - k5r\,SFK^*\,ZAPp) * 60$
$r6$	$((k6f1\,SFK^* + k6f2)CBP - k6r\,CBPp) * 60$
$r7$	$(k7f\,CBP\,CSK - k7r\,CSK^*) * 60$
$r8$	$((k8f1\,SFK^* + k8f2\,SFK^*\text{-}ZAPp)ZAPb - (k8r1\,SHP1^* + k8r2)ZAP^*) * 60$
$r9$	$((k9f1(ZAPp + ZAP^* + SFK^*\text{-}ZAPp) + k9f2\,SFK^* + k9f3\,SFK^*\text{-}ZAPp)ZAP^* - (k9r1\,SHP1^* + k9r2)ZAPp) * 60$
$r10$	$(k10f\,SFK^*\,SHP1 - k10r\,SHP1^*) * 60$
	LAT axis
$r11$	$k11f(ZAP^* + ZAPp + SFK^*\text{-}ZAPp)LAT - (k11r1\,SHP1^* + k11r2)LATp$
$r12$	$k12f\,LATp\,GRB2SOS - k12r\,SOSb$
$r13$	$k13f\,LATp\,PLC\gamma - k13r\,PLC\gamma p$
	CD28 axis
$r14$	$k14f\,CD28^*(ZAP^* + ZAPp + SFK^*\text{-}ZAPp)PI3K - k14r\,PI3K^*$
$r15$	$k15f\,PI3K^*\,PIP2 - (k15r1\,PTEN^* + k15r2)PIP3$
$r16$	$k16f\,PIP3\,PDK1 - k16r\,PDK1^*$
$r17$	$k17f1\,PDK1^* + k17f2\,mTORC2^* + k17f3\,PDK1^*\,mTORC2^*)AKT - k17r\,AKT^*$
$r18$	$k18f\,AKT^*\,TSC12 - k18r\,TSCp$
$r19$	$k19f\,TSC12\,RHEBgtp - k19r\,RHEBgdp$
$r20$	$k20f\,RHEBgtp\,mTORC1 - k20r\,mTORC1^*$
$r21$	$k21f\,PI3K^*\,mTORC2 - (k21r1\,mTORC1^* + k21r2)mTORC2^*$
$r22$	$k22f\,PTEN - k22r(TCRp^{n22r}/(TCRp^{n22r} + kr22^{n22r}))PTEN^*$

Table 2: The rate equations of the various signaling molecules within the model. Equations in ZAP axis are multiplied by 60 to account for time-scale differences in parameter values. Model equations adapted from Zheng et al. (2005) and Perley et al. (2014).

Parameter	Value	Units	Significance	Source
$TCRp$	20000	mol	Total number of phosphorylated receptor (model input)	Zheng et al. (2005)
ZAP_{total}	100000	mol	Quantity of ZAP70 in cell	Zheng et al. (2005)
SFK_{total}	120000	mol	Quantity of SFK in cell	Zheng et al. (2005)
$CD45_{total}$	100000	mol	Quantity of CD45 in cell	Zheng et al. (2005)
CBP_{total}	50000	mol	Quantity of CBP in cell	Zheng et al. (2005)
CSK_{total}	50000	mol	Quantity of CSK in cell	Zheng et al. (2005)
$SHP1_{total}$	1000000	mol	Quantity of SHP1 in cell	Zheng et al. (2005)
$k1f$	$2 \cdot 10^{-5}$	$(\text{mol} \cdot \text{s})^{-1}$	Association rate of ZAP70-TCR binding	Zheng et al. (2005)
$k1r$	$4.2 \cdot 10^{-2}$	s^{-1}	Dissociation rate of ZAP70-TCR binding	Zheng et al. (2005)
$k2f$	$4 \cdot 10^{-7}$	$(\text{mol} \cdot \text{s})^{-1}$	Phosphorylation rate of SFK	Zheng et al. (2005)
$k2r$	$4 \cdot 10^{-6}$	s^{-1}	Dephosphorylation rate of bound SFK	Zheng et al. (2005)
$k3f$	$4 \cdot 10^{-3}$	s^{-1}	Phosphorylation rate of SFK by other kinases	Zheng et al. (2005)
$k3r1$	$4 \cdot 10^{-6}$	$(\text{mol} \cdot \text{s})^{-1}$	Dephosphorylation rate of SFK* by CD45 or SHP1	Zheng et al. (2005)
$k3r2$	$8 \cdot 10^{-2}$	s^{-1}	Dephosphorylation rate of SFK* by other phosphatases	Zheng et al. (2005)
$k4f$	$5 \cdot 10^{-6}$	$(\text{mol} \cdot \text{s})^{-1}$	Association rate of ZAPp to SFK via SH2 domains	Zheng et al. (2005)
$k4r$	$8 \cdot 10^{-3}$	s^{-1}	Dissociation rate of ZAPp to SFK via SH2 domains	Zheng et al. (2005)
$k5f$	$8 \cdot 10^{-2}$	s^{-1}	Dissociation rate of ZAPp to SFK via SH2 domains	Zheng et al. (2005)
$k5r$	$1 \cdot 10^{-6}$	$(\text{mol} \cdot \text{s})^{-1}$	Association rate of ZAPp to SFK via SH2 domains	Zheng et al. (2005)
$k6f1$	$8.33 \cdot 10^{-7}$	$(\text{mol} \cdot \text{s})^{-1}$	Phosphorylation rate of SFK by SFK	Zheng et al. (2005)
$k6f2$	$1 \cdot 10^{-2}$	s^{-1}	Phosphorylation rate of SFK by other kinases	Zheng et al. (2005)
$k6r$	$8 \cdot 10^{-7}$	$(\text{mol} \cdot \text{s})^{-1}$	Dephosphorylation rate of SFK	Zheng et al. (2005)
$k7f$	$8.89 \cdot 10^{-7}$	$(\text{mol} \cdot \text{s})^{-1}$	Phosphorylation rate of CSK	Zheng et al. (2005)
$k7r$	$4 \cdot 10^{-2}$	s^{-1}	Dephosphorylation rate of CSK	Zheng et al. (2005)
$k8f1$	$4 \cdot 10^{-7}$	$(\text{mol} \cdot \text{s})^{-1}$	Tyrosine phosphorylation rate of bound ZAP by SFKdp	Manually derived
$k8f2$	$2.5 \cdot 10^{-6}$	$(\text{mol} \cdot \text{s})^{-1}$	Tyrosine phosphorylation rate of bound ZAP by SFK*	Zheng et al. (2005)
$k8r1$	$4 \cdot 10^{-}6$	$(\text{mol} \cdot \text{s})^{-1}$	Dephosphorylation rate of ZAP* by SHP1	Zheng et al. (2005)
$k8r2$	$8 \cdot 10^{-2}$	s^{-1}	Dephosphorylation rate of ZAP* by other phosphatses	Zheng et al. (2005)
$k9f1$	$4.44 \cdot 10^{-6}$	$(\text{mol} \cdot \text{s})^{-1}$	Tyrosine phosphorylation rate of ZAP* by activated ZAP	Zheng et al. (2005)
$k9f2$	$8.33 \cdot 10^{-7}$	$(\text{mol} \cdot \text{s})^{-1}$	Tyrosine phosphorylation rate of ZAP* by SFKdp	Zheng et al. (2005)
$k9f3$	$2.5 \cdot 10^{-6}$	$(\text{mol} \cdot \text{s})^{-1}$	Tyrosine phosphorylation rate of ZAP* by SFK*	Zheng et al. (2005)
$k9r1$	$4 \cdot 10^{-6}$	$(\text{mol} \cdot \text{s})^{-1}$	Dephosphorylation rate of ZAPp by SHP1	Zheng et al. (2005)
$k9r2$	$8 \cdot 10^{-2}$	s^{-1}	Dephosphorylation rate of ZAPp by other phosphatases	Zheng et al. (2005)
$k10f$	$8.64 \cdot 10^{-10}$	$(\text{mol} \cdot \text{s})^{-1}$	Activation rate of SHP1	Zheng et al. (2005)
$k10r$	$4 \cdot 10^{-4}$	s^{-1}	Deactivation rate of SHP1	Zheng et al. (2005)
$k11f$	$4 \cdot 10^{-8}$	$(\text{mol} \cdot \text{s})^{-1}$	Activation rate of CD45	Zheng et al. (2005)
$k11r$	$2 \cdot 10^{-4}$	s^{-1}	Deactivation rate of CD45	Zheng et al. (2005)

Table 4: Parameter values of the ZAP axis; adapted from Zheng et al. (2005) and Perley et al. (2014).

Parameter	Value	Units	Significance	Source
LAT_{total}	50000	mol	Quantity of LAT in cell	Perley et al. (2014)
$PLC\gamma_{total}$	50000	mol	Quantity of PLCγ in cell	Perley et al. (2014)
$GRB2SOS_{total}$	50000	mol	Quantity of GRB2SOS in cell	Perley et al. (2014)
$PIP2_{total}$	10000000	mol	Quantity of PIP2 in cell	Perley et al. (2014)
$k12f$	$3 \cdot 10^{-4}$	$(\text{mol} \cdot \text{min})^{-1}$	Phosphorylation rate of LAT by activated ZAP	Perley et al. (2014)
$k12r1$	$2 \cdot 10^{-3}$	$(\text{mol} \cdot \text{min})^{-1}$	Dephosphorylation rate of LAT by activated SHP1	Perley et al. (2014)
$k12r2$	$9 \cdot 10$	min^{-1}	Dephosphorylation rate of LAT by other phosphatases	Perley et al. (2014)
$k13f$	$3 \cdot 10^{-3}$	$(\text{mol} \cdot \text{min})^{-1}$	Association rate of PLCγ to LAT complex	Perley et al. (2014)
$k13r$	$3 \cdot 10^{2}$	min^{-1}	Dissociation rate of PLCγ from LAT complex	Perley et al. (2014)
$k14f$	$3 \cdot 10^{-5}$	$(\text{mol} \cdot \text{min})^{-1}$	Association rate of SOSb to LAT complex	Perley et al. (2014)
$k14r$	$6 \cdot 10^{-2}$	min^{-1}	Dissociation rate of SOSb from LAT complex	Perley et al. (2014)

Table 6: Parameter values of the LAT axis; adapted from Zheng et al.Zheng et al. (2005) and Perley et al.Perley et al. (2014).

Parameter	Value	Units	Significance	Source
$CD28^*$	20000	mol	Total number of activated co-receptor (input signal)	Manually derived
$PI3K_{total}$	10000	mol	Quantity of PI3K in cell	Perley et al. (2014)
$PDK1_{total}$	10000	mol	Quantity of PDK1 in cell	Perley et al. (2014)
AKT_{total}	10000	mol	Quantity of AKT in cell	Perley et al. (2014)
TSC_{total}	10000	mol	Quantity of TSC in cell	Perley et al. (2014)
$RHEB_{total}$	10000	mol	Quantity of RHEB in cell	Perley et al. (2014)
$mTORC1_{total}$	10000	mol	Quantity of mTORC1 in cell	Perley et al. (2014)
$mTORC2_{total}$	10000	mol	Quantity of mTORC2 in cell	Perley et al. (2014)
$PTEN_{total}$	10000	mol	Quantity of PTEN in cell	Perley et al. (2014)
$k15f$	$3 \cdot 10^{-9}$	$(\text{mol}^2 \cdot \text{min})^{-1}$	Activation rate of PI3K by activated CD28	Perley et al. (2014)
$k15r$	$3 \cdot 10$	min^{-1}	Dissociation rate of PI3K	Perley et al. (2014)
$k16f$	3	$(\text{mol} \cdot \text{min})^{-1}$	Phosphorylation rate of PIP2 by PI3K	Perley et al. (2014)
$k16r1$	$3 \cdot 10$	$(\text{mol} \cdot \text{min})^{-1}$	Dephosphorylation rate of PIP3 by PTEN	Perley et al. (2014)
$k16r2$	$1 \cdot 10^{-10}$	min^{-1}	Dephosphorylation rate of PIP3 by other phosphatases	Perley et al. (2014)
$k17f$	$3 \cdot 10^{-5}$	$(\text{mol}^2 \cdot \text{min})^{-1}$	Activation rate of PDK1 by PIP3	Perley et al. (2014)
$k17r$	$3 \cdot 10$	min^{-1}	Dissociation rate of $PDK1^*$	Perley et al. (2014)
$k18f1$	$1 \cdot 10^{-8}$	$(\text{mol} \cdot \text{min})^{-1}$	Phosphorylation rate of AKT by $PDK1^*$	Manually derived
$k18f2$	$1 \cdot 10^{-11}$	$(\text{mol} \cdot \text{min})^{-1}$	Phosphorylation rate of AKT by $mTORC2^*$	Manually derived
$k18f3$	$1 \cdot 10^{-8}$	$(\text{mol}^2 \cdot \text{min})^{-1}$	Phosphorylation rate of AKT by $PDK1^*$ and $mTORC2^*$	Perley et al. (2014)
$k18r$	$1 \cdot 10^{-1}$	min^{-1}	Dephosphorylation rate of AKT	Manually derived
$k19f$	$1 \cdot 10$	$(\text{mol} \cdot \text{min})^{-1}$	Phosphorylation of TSC2 subunit of TSC1-2 complex	Perley et al. (2014)
$k19r$	1	min^{-1}	Association of TSC2 to TSC1	Perley et al. (2014)
$k20f$	$1 \cdot 10^{-4}$	$(\text{mol} \cdot \text{min})^{-1}$	Activation rate of RHEBgtp	Perley et al. (2014)
$k20r$	$1 \cdot 10^{-1}$	min^{-1}	Dissociation rate of RHEBgtp	Manually derived
$k21f$	$1 \cdot 10^{-4}$	$(\text{mol} \cdot \text{min})^{-1}$	Activation rate of mTORC1 by RHEBGTP	Perley et al. (2014)
$k21r$	1	min^{-1}	Dissociation rate of mTORC1 by RHEBGTP	Perley et al. (2014)
$k22f$	$3 \cdot 10^{-3}$	$(\text{mol} \cdot \text{min})^{-1}$	Activation rate of mTORC2 by $PI3K^*$	Perley et al. (2014)
$k22r1$	$3 \cdot 10^{-3}$	$(\text{mol} \cdot \text{min})^{-1}$	Dissociation rate of mTORC2 by $mTORC1^*$	Perley et al. (2014)
$k22r2$	3	min^{-1}	Dissociation rate of mTORC2 by other phosphatases	Perley et al. (2014)
$k23f$	1	$(\text{mol} \cdot \text{min})^{-1}$	Activation rate of PTEN	Perley et al. (2014)
$k23r$	$2 \cdot 10$	min^{-1}	Deactivation rate of $PTEN^*$ by TCR complex	Perley et al. (2014)
$n23r$	$1 \cdot 10$		$PTEN^*$ hill coefficient of deactivation	Perley et al. (2014)
$kr23$	$0.75 \cdot TCRp$	mol	Quantity of TCRp producing half maximum $PTEN^*$ deactivation	Perley et al. (2014)

Table 8: Parameter values of the CD28 axis; adapted from Zheng et al.Zheng et al. (2005) and Perley et al.Perley et al. (2014).

6.2. Defining a valid parameter space for the model

With the parameterization of the model described in Zheng et al. (2005) and Perley et al. (2014), the model is able to produce intrinsic oscillatory signals, shown in Fig. S1. For instance, setting $TCRp = 20000$ mol and $k7f = 4.89 \cdot 10^{-7}\,(\text{mol} \cdot \text{s})^{-1}$ and plotting the one-parameter bifurcation of $ZAPp$ with respect to $k10f$ (the rate constant for $SHP1$ activation), as shown in Fig. S1(A), produces a diagram that effectively eliminates the bistable behavior of the model and produces an oscillatory regime defined by the envelopes of stable limit cycles initiated from the saddle-node of periodic orbits (SNP) and terminate at a saddle-node on an invariant circle (SNIC) bifurcation (formed by SN2 and a homoclinic bifurcation HM). The stable envelopes of limit cycles produce periodic solutions whose time series simulations exhibit periodic spiking in ZAP_{active}, as shown in Fig. S1(B). This spiking pattern in ZAP_{active} has not been observed experimentally, indicating that this is a non-viable parameter regime of the model. Phys-

iologically, since $ZAP70$ remains bound to the TCR throughout antigen presentation, this spiking pattern suggests that $ZAP70$ is repeatedly getting phosphorylated and subsequently dephosphorylated in the time scale of seconds, all while remaining bound to the phosphorylated TCR (via the non-zero $TCRp$ parameter). This result contradicts the literature showing a continuous level of phosphorylated $ZAP70$ throughout antigen stimulation Houtman et al. (2005); An et al. (2019). The lack of evidence showing a spiking $ZAP70$ pattern as well as the contrast to experimentally observed $ZAP70$ binding/unbinding kinetics leads us to designate this regime as an invalid result of the model, as this behaviour is unlikely to exist. To resolve this issue, we have developed a systematic framework to eliminate this oscillatory regime while maintaining the other model regimes. This is the focus of the following section.

6.3. Eliminating the intrinsic oscillatory regime

This approach is adapted from the Dynamics Visualisation based on Parallel Coordinates (DYVIPAC) framework by Nguyen et al. (2015). Broadly, it involves a population-based approach to uncover system's dynamics. The m parameters whose effects on model dynamics we are interested in are first selected, and a range of values for each parameter is set. A sample of n model realizations (i.e. simulated steady state response) is then created, each with a randomly selected parameterization from within the pre-determined ranges. These realizations are integrated starting from the same initial conditions, and their steady state solution is classified according to its dynamics. A parallel coordinates plot is then created linking each realization of the model to its respective steady state classification. This allows us to obtain a multi-dimensional view of model dynamics, and allows us to reliably identify parameter regimes where the oscillatory solution exists. By limiting our parameter sampling ranges to exclude such parameter regimes, the oscillatory solutions can be excluded from our model. This approach is explored in more detail in the following sections.

6.3.1. Network model and parameter selection

The first step of this framework is to identify the parameters of interest, or more specifically those that we vary in this study. These parameters are $TCRp$ and $k10f$; $k8f1$ is also selected since it allows us to more easily eliminate the oscillatory regime. The number of parameters defines the dimensionality m of this approach (i.e., $m = 3$).

6.3.2. Parameter sampling

With the dimensionality m of the framework determined through parameter selection, an appropriate sampling range of these parameters now needs to be set. Each realization of the model will have a randomly selected value, selected from within this range. Since we are interested in the effect of the circadian rhythm, this parameter range should include the degree of modulation due to the circadian rhythm. This range is therefore defined by

$$p_i \in [p_{i,min}, p_{i,max}], \tag{4}$$

where p_i is the the value of a parameter i randomly sampled from within a set range. This p_i, when sampled over a sufficiently large k realizations, demonstrates all the possible values this parameter can have when subjected to a circadian rhythm. $p_{i,0}$ denotes the default parameter value, and $p_{i,min}$ and $p_{i,max}$ denote the minimum and maximum endpoints from which this parameter can be sampled from.

6.3.3. Setting a physiological p_i range

To impose a physiologically-relevant limit for the influence of the circadian rhythm, we note that in CD8$^+$ T cell signaling it was shown that IFNγ, along with other CD8$^+$ T cell cytokines, approximately vary within a $[0.5 \times p_0, 1.5 \times p_0]$ range depending on the time of initial vaccination (Fortier et al., 2011; Nobis et al., 2019). We will therefore use this range to describe the influence of the circadian rhythm on CD8$^+$ T cell signaling. To produce this p range, we choose the range of viable circadian coefficient α to be $\alpha \in [0, 0.5]$. It should be noted that this only defines the maximum range of p; some realizations of the model may have a parameter subjected to a weaker circadian influence (defined by an $\alpha < 0.5$).

It is also important to note that the above range assumes that a $[0.5 \times p_0, 1.5 \times p_0]$ discrepancy in cytokine production can be traced linearly to a discrepancy of a similar magnitude in ZAP signaling. While we show in this study that the axes downstream of ZAP do not contribute significantly to model dynamics, we acknowledge that there may be additional factors contributing to the discrepancy experimentally seen in IFNγ and other cytokines. Regardless, this assumption is made in this study to facilitate our analysis and selection of a viable parameter range.

6.4. Analysis of dynamical behaviour

With k model realizations selected from parameters within physiological ranges, the individual realizations can be integrated and their steady-state solution analyzed and classified according to its properties. Whereas DYVIPAC uses model eigenvalues to calculate stability (Nguyen et al., 2015), our approach classifies solutions based on their steady state behaviour. Namely, we classify solutions as either elevated (i.e., corresponding to those with a higher than 5% active ZAP concentration), oscillatory (i.e., corresponding to those with a slope greater than a manually selected threshold of 0.0053) or inactive (i.e., corresponding to those fulfilling neither of the previous criteria). We have found that performing the classification in this manner is effective due to two important dynamic features of the model, including: (i) its fast dynamics, allowing it to reach steady state relatively quickly, and (ii) the relaxation oscillation-like behaviour it exhibits within the oscillatory regime with its rapid up and down-stroke oscillations that facilitate our ability to classify it according to its slope.

With this, we are left with a matrix of k model realizations, each with its unique paramaterization of the m circadian-affected parameters, and with a label designating the classification of each k_i solution based on the properties of its steady-state dynamics.

6.5. Parallel coordinate plot visualization

This dataset is visualized using a parallel coordinate plot, which displays how these different parameter values can influence the dynamics of the model. Each model realization is linked to its respective steady state dynamics according to the value of its parameters of interest. This visualization is shown in Figure S2(A), where a multi-dimensional analysis of three parameters, including $TCRp$, $k10f$ (which represents SHP1 activation) and $k8f1$ (which represents ZAP activation), is conducted. In this analysis, $k = 1000$ model realizations are used, where each realization is represented individually by a colored segmented line linking the parameter values generating this realization. The parameter values of each realization lie above the ticks on the x-axis representing each parameter, and are connected by a segmented line color-coded according to the stability property of that particular model realization (i.e., the stability of the steady-state solution associated with that realization). Three colors are used, blue, red and yellow representing inactive, elevated and oscillatory solutions, respectively.

The parameter values are scaled between $[0, 1]$ according to their respective maximum and minimum sample values. This normalization is generated using the equation

$$p_{i,norm} = \frac{p_i - p_{i,min}}{p_{i,max} - p_{i,min}} \tag{5}$$

where, $p_{i,norm}$ is the normalized parameter value between $[0, 1]$ of a specific parameter of interest. p_i is the parameter value of a particular model realization, and $p_{i,max}$ and $p_{i,min}$ are the respective maximum and minimum parameter values across all n realizations. This visualization allows us to obtain a broader picture of model dynamics and how these dynamics can be shaped by different parameter combinations.

6.5.1. Eliminating the oscillatory regime

Using the parallel coordinate plot, the oscillatory regime can be extracted from the original scaled range of an indicator parameter p_i by removing the continuous interval within this range associated with the oscillatory behaviour (i.e., the interval that has segmented yellow lines). The indicator parameter p_i is then re-scaled according to the remaining interval and sampling is then restricted to this constrained range (which by design excludes oscillatory solutions). This is done in Fig. S2(B), where the elevated and inactive solutions from the previously presented parallel coordinate plot are hidden, to better visualize the oscillatory regimes.

We identify that oscillatory solutions seem to be confined to a normalized $k8f1$ range of $[0.23, 1]$ of $k8f1$. Thus, by only sampling from $k8f1 \in [0, 0.23]$, the oscillatory regime can be completely avoided.

Using this threshold of $k8f1_{max} = 0.23\,(\mathrm{mol} \cdot \mathrm{s})^{-1}$, we reverse the previously described normalization process, to obtain the raw maximum value of $k8f1_{max} = 6.12\,(\mathrm{mol} \cdot \mathrm{s})^{-1}$. To obtain the new $p_{i,0}$ for $k8f1$, the trivial calculation of $p_{i,0} = k8f1_{max}/1.5$ is performed. The preceding calculation is repeated to find $k8f1_{min}$, thus producing a new range $k8f1 \in [2.72, 6.12]\,(\mathrm{mol} \cdot \mathrm{s})^{-1}$. Applying parallel coordinate plot on this new regime now only produces two outcomes: the inactive and elevated states, as shown in Figure S2. Through this new $k8f1$ parameterization, we observe that the oscillatory regime is indeed eliminated, while still preserving both the inactive and elevated model solution. Thus, this new model parameterization can safely allow us to simulate the effects of the circadian rhythm on $CD8^+$ T cell signaling without worrying about intrinsic oscillatory dynamics that could be produced by the model; this is because we are certain that any com-

bination of these three parameters under this parameterization considered in Figure S2(C) would not produce the non-viable oscillatory solutions.

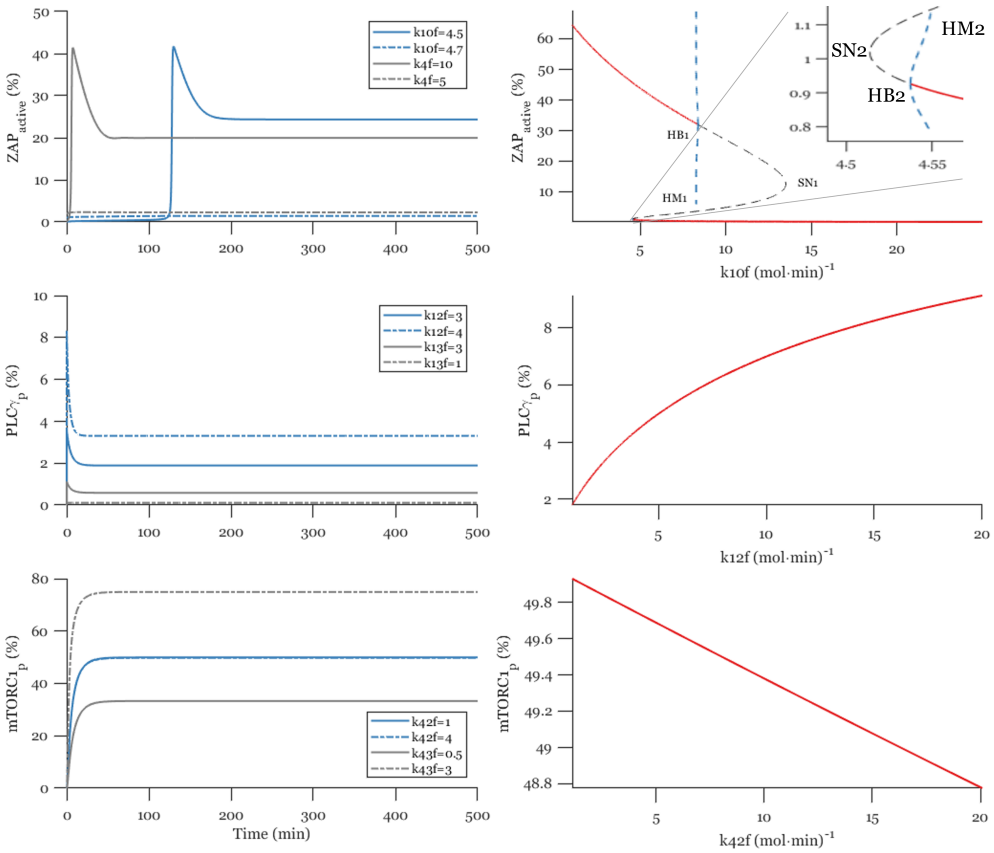

Figure 2: (A) Time series simulations of ZAP_{active}, the output of the ZAP axis, at different values of $k10f$ and $k4f$ specified in the legend, where $k10f$ & $k4f$ are the parameters for $SHP1$ phosphorylation SFK^* and $ZAPp$ binding, respectively. (B) One-parameter bifurcation of ZAP_{active} with respect to $k10f$. Red (gray) solid (dashed) lines represent stable (unstable) branches of equilibria, while blue dashed lines represent envelopes of unstable limit cycles emerging from Hopf bifurcations (HB1 and HB2) and terminating at homoclinic bifurcations (HM1 and HM2). SN1 and SN2: saddle-node bifurcations. (C) Time series simulations of $PLC\gamma p$ as a percentage relative to its total concentration: $PLC\gamma + PLC\gamma p$, at different values of $k12f$ and $k13f$ specified in the legend, where $k12f$ and $k13f$ are the forward rate constants of LAT and $PLC\gamma$ phosphorylation, respectively. (D) One-parameter bifurcation of $PLC\gamma p$ percentage with respect to $k12f$. Red line represents branch of stable equilibria. (E) Time series simulations of $mTORC1^*$ as a percentage relative to its total concentration: $mTORC1 + mTORC1^*$, at different values of $k42f$ and $k43f$ specified in the legend, where $k42f$ and $k43f$ are the forward rate constants of $RhebGDP$ and $mTORC1$ activation, respectively. (D) One-parameter bifurcation of $mTORC1^*$ percentage with respect to $k42f$. Red line represents branch of stable equilibria. All time series simulations and bifurcation diagrams are plotted with $TCRp = 27000$ mol; for all other parameter values, see Table 6.1.

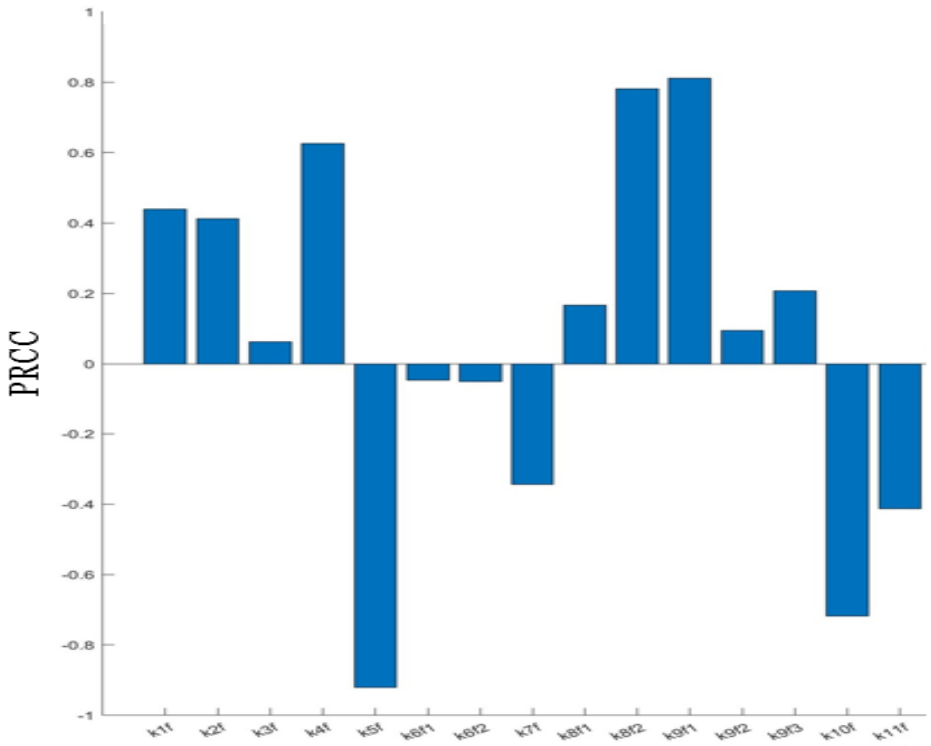

Figure 3: Partial rank correlation coefficients (PRCC) of the activation parameters of the ZAP axis when correlated to ZAP_{active} output. A higher PRCC value indicates a higher correlation between values of that parameter with ZAP_{active} (positively correlated if PRCC > 0, negatively correlated if PRCC < 0). The following parameters $k4f, k5f, k8f2, k9f1$ and $k10f$ are identified as sensitive with correlation coefficients $> |0.6|$.

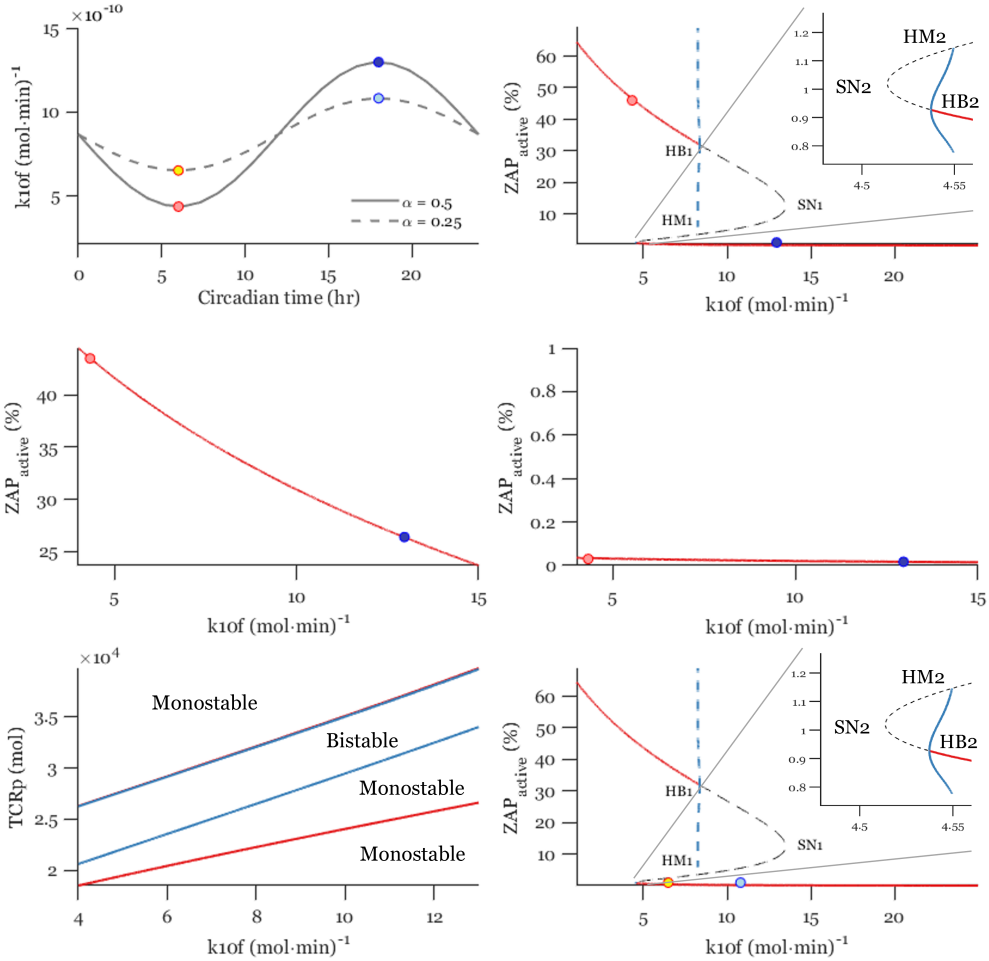

Figure 4: (A) Time series plots of $k10f_t$ when $\alpha_{k10f} = 0.5$ (solid line) and $\alpha_{k10f} = 0.25$ (dashed line) showing 24 hr cycles with different amplitudes. Orange (yellow) and blue (light blue) dots show the diurnal maxima and minima of $k10f_t$ when $\alpha_{k10f} = 0.5$ ($\alpha_{k10f} = 0.25$). (B) One-parameter bifurcation of ZAP_{active} with respect to $k10f$ at $TCRp = 27000$ mol. Details of the bifurcation diagram are described in Fig. 2. Orange and blue superimposed dots represent the respective day and night extrema of $k10f_t$ identified in (A). Note the abrupt change in steady state upon crossing HB1 and HB2. (C), (D) One-parameter bifurcation of ZAP_{active} with $TCRp = 40000$ mol (C) and $TCRp = 10000$ mol (D). Note the monostable response across the $k10f_t$ parameter space. (E) Two-parameter bifurcation of ZAP_{active} with respect to $k10f$ and $TCRp$. Red lines denote continuations of saddle-node bifurcations (SN1 and SN2), while blue lines denote continuations of the Hopf bifurcations (HB1 and HB2). Bistability is bounded by HB1 and HB2. (F) one-parameter bifurcation of ZAP_{active} at $TCRp = 27000$ mol as in (B), but with $\alpha_{k10f} = 0.25$; the day-night maxima identified in (A) are superimposed as yellow and light blue dots.

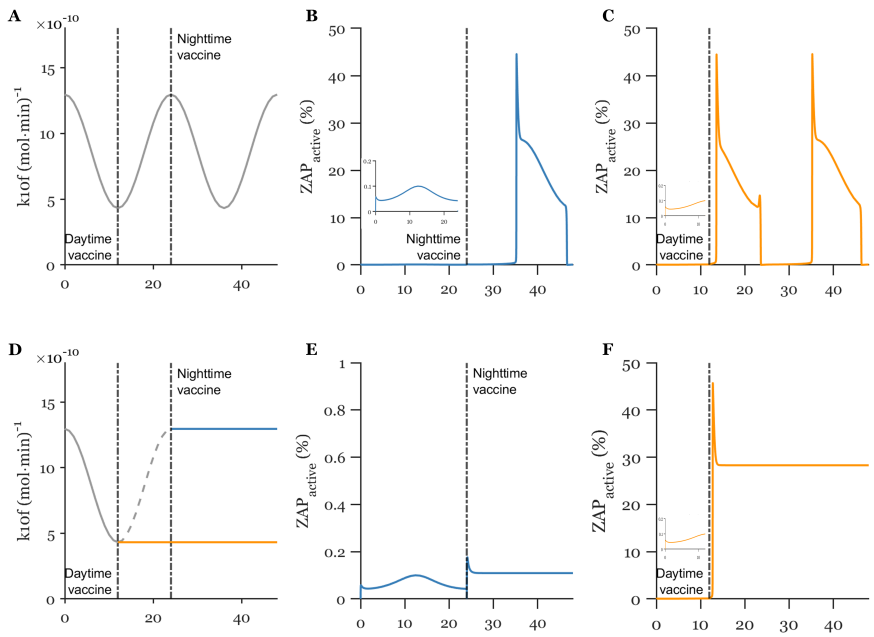

Figure 5: (A) Time series plot of $k10f_t$ when $\alpha_{k10f} = 0.5$ showing 24 hr cycles. Dashed-dotted lines indicate the moments of vaccine applications at daytime ($t = 12$ hr) and at nighttime ($t = 24$ hr). (B) Time series simulations of ZAP_{active} prior and post vaccination applied at nighttime ($t = 24$ hr). Inset: magnification of the time series simulations prior to vaccination to highlight the small amplitude oscillations associated with the state S_0. (C) Time series simulations of ZAP_{active} prior and post vaccination applied at daytime ($t = 12$ hr). Notice the repetitive large amplitude oscillations associated with the state S_1 produced post vaccination at nighttime and daytime; the onset of the large amplitude oscillations in the former case (nighttime vaccination) is delayed relative to the latter case (daytime vaccination). (D) Time series plot of $k10f_t$ when $\alpha_{k10f} = 0.5$ showing 24 hr cycles that get interrupted upon vaccination at daytime (orange; 12 hr) and nighttime (blue; 24 hr). When vaccination is applied in each case, $k10f_t$ is then kept steady at its respective value. (E) Time series simulations of ZAP_{active} prior and post vaccination applied at nighttime ($t = 24$ hr). (C) Time series simulations of ZAP_{active} prior and post vaccination applied at daytime ($t = 12$ hr). Inset: magnification of the time series simulations prior to vaccination to highlight the small amplitude oscillations associated with the state S_0. Notice the much larger response associated with S_1 produced post vaccination at daytime compared to nighttime, as well as the absence of oscillations post vaccination in both cases.

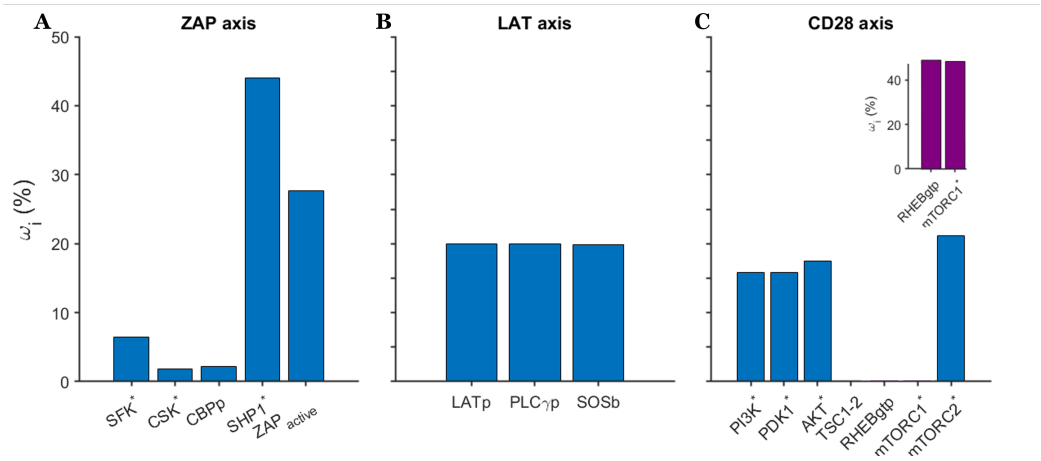

Figure 6: Bar plots of the magnitude of the oscillatory contribution ω_i for different molecular players within the (A) ZAP axis, (B) LAT axis, and (C) CD28 axis when $k10f_t$ is oscillatory with $\alpha_{k10f} = 0.5$. The larger the ω_i value, the stronger the influence of the circadian-induced oscillations have on the steady state level of the molecular player i of interest. Inset in panel (C): Bar plots of the magnitude of the oscillatory contribution ω_i for the molecular players $i = RhebGTP$ and $mTORC1^*$ within the CD28 axis when $k42f_t$ is oscillatory with $\alpha_{k42f} = 0.5$.

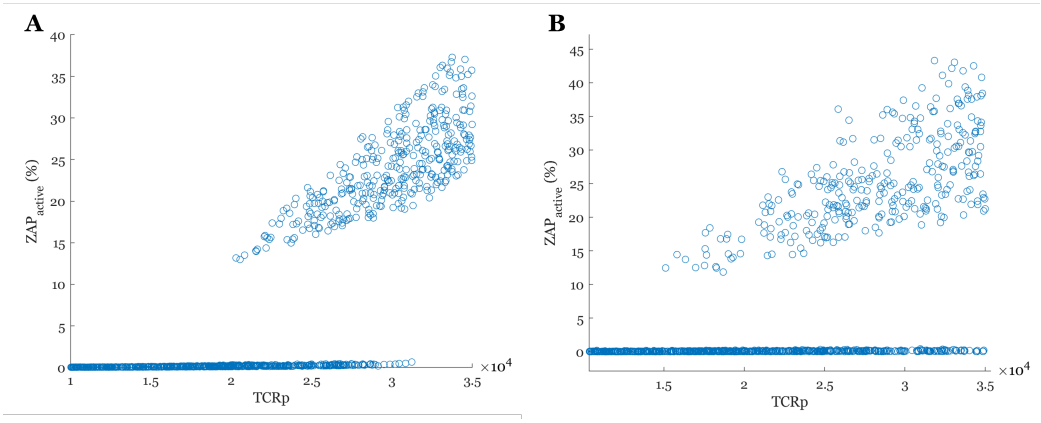

Figure 7: Macro-bifurcation diagram of ZAP_{active} with respect to $TRCp$ when various combinations of circadian-affected parameters are assigned random values within their respective ranges: (A) $k10f$ is randomly assigned values within the range $[0.5 \times k10f_0, 1.5 \times k10f_0]$. (B) $k4f, k9f1, k8f1, k11f, k7f, k10f$ are randomly assigned values within the ranges $[0.5 \times par_0, 1.5 \times par_0]$, where $par = k4f, k9f1, k7f, k10f, k11f, k8f1$.

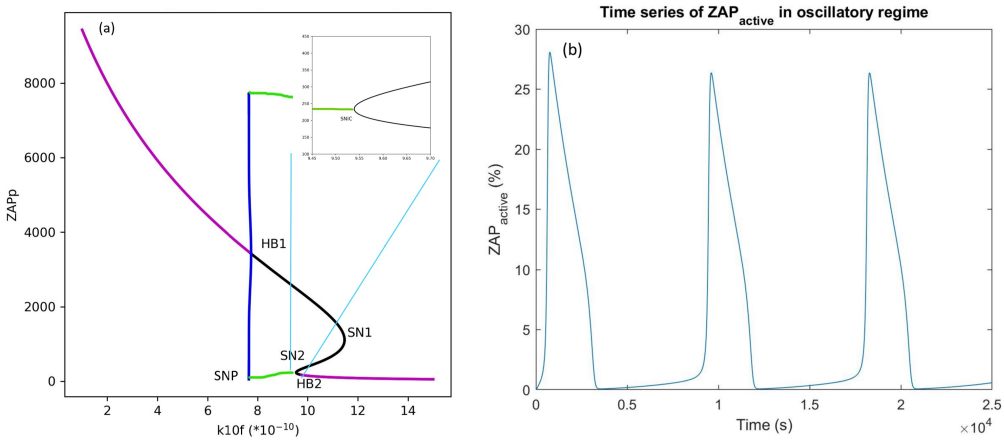

Figure S1: (A) One-parameter bifurcation of phosphorylated ZAP ($ZAPp$) with respect to $k10f$ when $TCRp = 20000$ mol and $k7f = 4.89 \cdot 10^{-7}$ $(\text{mol} \cdot \text{s})^{-1}$. Red solid (gray dashed) lines represent stable (unstable) branches of equilibria, while blue solid (dashed) lines represent envelopes of stable (unstable) limit cycles. HB1 and HB2: Hopf bifurcations, HM1 and HM2: homoclinic bifurcations, SN1 and SN2: saddle-node bifurcations, SNP: saddle-node of periodics bifurcation, SNIC: saddle-node on an invariant circle bifurcation formed by SN2 and HM1 (see inset for magnification). Note that the periodic continuation (green) was superimposed afterwards due to a lack of convergence. (B) A time series simulation of an oscillatory solution of ZAP_{active} obtained by setting $TCRp = 20000$ mol, $k7f = 4.89 \cdot 10^{-7}$ $(\text{mol} \cdot \text{s})^{-1}$ and $k10f = 9 \cdot 10^{-10}$ $(\text{mol} \cdot \text{s})^{-1}$.

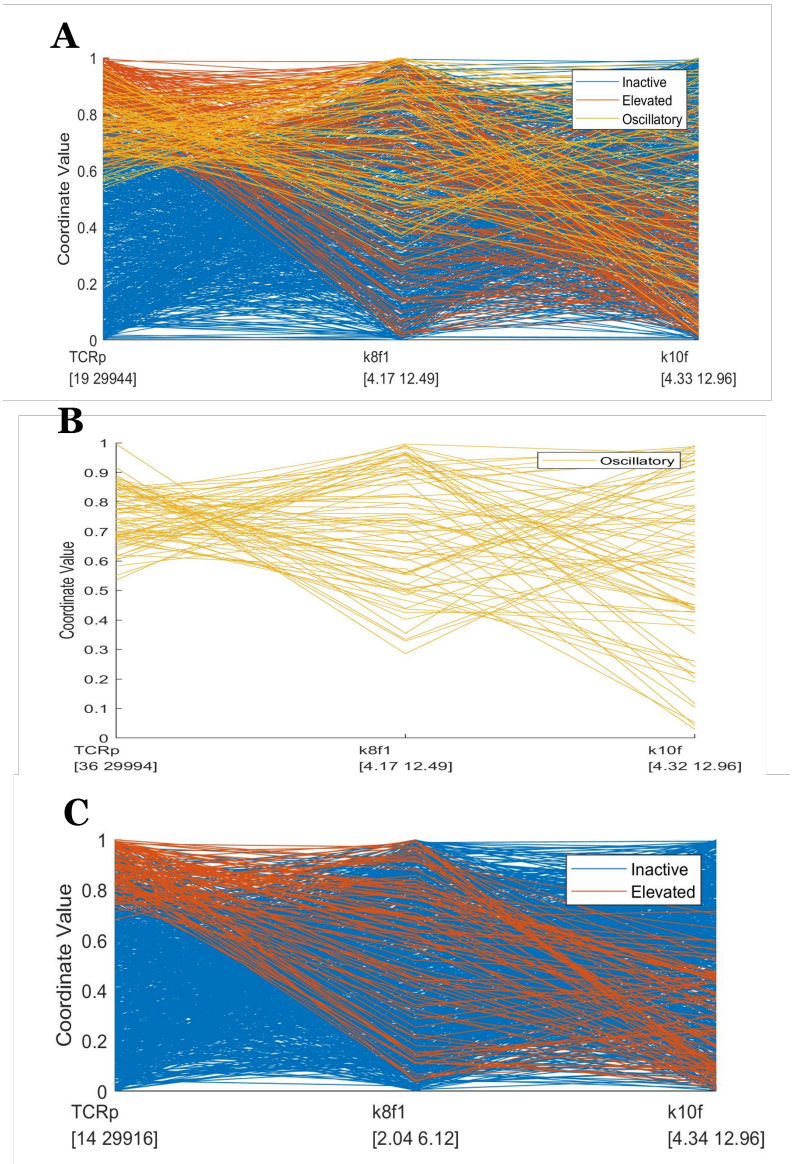

Figure S2: Parallel coordinate plot of $TCRp, k8f1, k10f$. (A) The three parameters are displayed on the x-axis and their normalized parameter values are displayed on the y-axis. Each segmented colored line represents a given model realization (steady state response) sampled randomly from within a pre-determined range. The segmented lines are color-coded according to the type of steady state obtained: blue for inactive, red for elevated and yellow for oscillatory solution. (B) The isolated oscillatory solutions (yellow) from (A). (C) The analysis repeated with a constrained parameter range for $k8f1$. Notice the lack of yellow oscillatory solutions.